Stanford | SCHOOL OF EARTH, ENERGY & ENVIRONMENTAL SCIENCES

DEPARTMENT OF GEOPHYSICS

May 24, 2019

Dr. Paolo Tarolli
Viale dell'Universita, 16
35020 Legnaro PD, Italy

Dear Dr. Tarolli,

This letter accompanies the submission of the REVISED manuscript NHESS-2018-347 entitled, "What's streamflow got to do with it? A probabilistic simulation of the competing oceanographic and fluvial processes driving extreme along-river water levels." We have thoroughly considered and addressed the comments of the reviewers, and feel that this enabled us to better explain and clarify the overall framework and the importance of our results, strengthening the overall manuscript.

Please find reviewer comments given in verbatim and our replies in italics. References to locations in the article are made by section (e.g., S3.5) or line number corresponding to the updated manuscript. The re-revised manuscript, which includes 14 figures, a supplemental information section, and this letter, has been uploaded.

Thank you for your consideration. Please contact me at kserafin@stanford.edu with any questions.

Sincerely,

Katherine A. Serafin (lead and corresponding author)
Postdoctoral Research Fellow
Stanford University

Anonymous Referee #1 Received and published: 4 March 2019

General comments

Serafin et al present a new framework for examining the joint influence of several coastal and riverine processes on water levels in estuarine environments, and show very clearly that the 100-yr ocean or 100-yr streamflow event does not always produce the 100-yr along-river water level. It is a novel piece of work using a clever methodological framework, resulting in an analysis that can assesses non-stationary water levels from a multivariate joint distribution and truly decompose coastal water levels. As such, I believe that the research forms an important contribution to the increasingly important field of compound flood risk assessment. The manuscript is well written in terms of language, but parts of it feel to long or could be helped by restructuring. There are also some specific methodological issues that require further explanation, as described in the following review. Nevertheless, if these can be sufficiently responded to, I believe that this paper would provide a very valuable addition to the literature.

Thank you!

Main comments

The introduction is generally well written and reviews most of the relevant literature. However, some important concepts for the paper are not fully introduced or defined. For example, a formal definition of compound flooding is missing. On page 2, line 20 (and also later at page 25, line 15) the authors imply that probabilistic simulations of water levels have not yet been done considering ocean and onland processes, and that this has only been done for specific events. However, Bevacqua et al (2017) van den Hurk et al. (2015), and Couasnon et al. (2018) have used probabilistic simulations. The current paper certainly adds value to the research carried out in those studies, but it would be prudent to mention them and how the current study advances.

We thank the reviewer for pointing out this oversight. We have added a formal definition of a compound event in the first line of the introduction, Page 1, Lines 16-17, "Coincident or compound events are a combination of physical processes in which the individual variables may or may not be extreme, however the result is an extreme event with a significant impact (Zscheischler et al., 2018, Bevacqua et al., 2017, Wahl et al., 2015, Leonard et al., 2014)." We have also added a brief description to the abstract, Page 1, Lines 1 -2, "Extreme water levels generating flooding in estuarine and coastal environments are often driven by compound events, where many individual processes such as waves, storm surge, streamflow, and tides coincide."

We thank the reviewer for noting that our writing seemed to imply that we were the first to produce probabilistic simulations of discharge and coastal water level events. Our intent was to highlight the novelty of the hybrid methodology merging physical and statistical models for return level analysis – which at the time the manuscript was completed and submitted was a novel application. However, after submission, Couasnon et al., 2018 and Moftakhari et al., 2019 published complementary frameworks. We thank the reviewer for suggesting the additional references, and have included the following text in our introduction to highlight the variety of previous studies, Page 2, Lines 22 – 28, "On the other hand, statistical models allow

Department of Geophysics
397 Panama Mall, Mitchell Earth Sciences Building, Stanford, CA 94305 T 650.497.6509

for the investigation of compound water levels through the simulation of combinations of dependent events which may not have been physically realized in observational records (Bevacqua et al., 2017, van den Herk et al., 2015). In addition, researchers have recently begun to generate hybrid models that link statistical and physical modeling approaches for understanding compound flood events (Moftakhari et al., 2019, Couasnon et al., 2018). Similar to the results solely from hydrodynamic and hydraulic models, statistical and hybrid modeling strategies show that simplifications of the dependence between multiple forcings may lead to an underestimation of flood risk."

In terms of the overall structure, the methods section (section 3, but also parts of section 4) are sometimes difficult to follow. The really interesting part here is the new overall framework. However, this overall framework sometimes gets lost in the details of the various specific models used, which can be rather lengthy (e.g. the part on HEC-RAS). It would be beneficial to the reader to highlight the overall methodological framework more clearly at the start of the methods section, for example with a flowchart. This would highlight more clearly the major novelty of this paper. It is of course also necessary to give details of the various components used for each part of the framework, such as HEC-RAS. But by emphasizing more the framework, it would be clear that one could also use the overall assessment framework with other hydrodynamic models, if one wished to do so.

Following on, it may help to move some of the details to Supplementary Information. General background information about setting up HEC-RAS can be shortened, and the essential parts for this study could be moved to supplementary information. This would improve overall readability of this section.

Related to the previous comments on structure, the part on HEC-RAS model validation (3.2.1) seems out of place in the methods section. It could be moved to the section on validation or in my opinion better to still to supplementary information.

We thank the author for the suggestions on how to better emphasize our framework. We have added a flowchart schematic that we hope better explains our hybrid modeling technique in the revised manuscript (Figure 3 in the manuscript, below as Figure 1). We agree that the amount of detail presented in the original manuscript may have added unnecessary length and detracted from the main value of the paper. In the revised manuscript, we have moved the sections describing the HEC-RAS model domain setup, validation and calibration to the Supplemental Information. We also have moved the section describing the tide gauge merging and removal of the river-influenced water levels to the Supplemental Information. We streamlined many of the sections and believe we have improved the overall readability of the manuscript.

Department of Geophysics
397 Panama Mall, Mitchell Earth Sciences Building, Stanford, CA 94305 T 650.497.6509

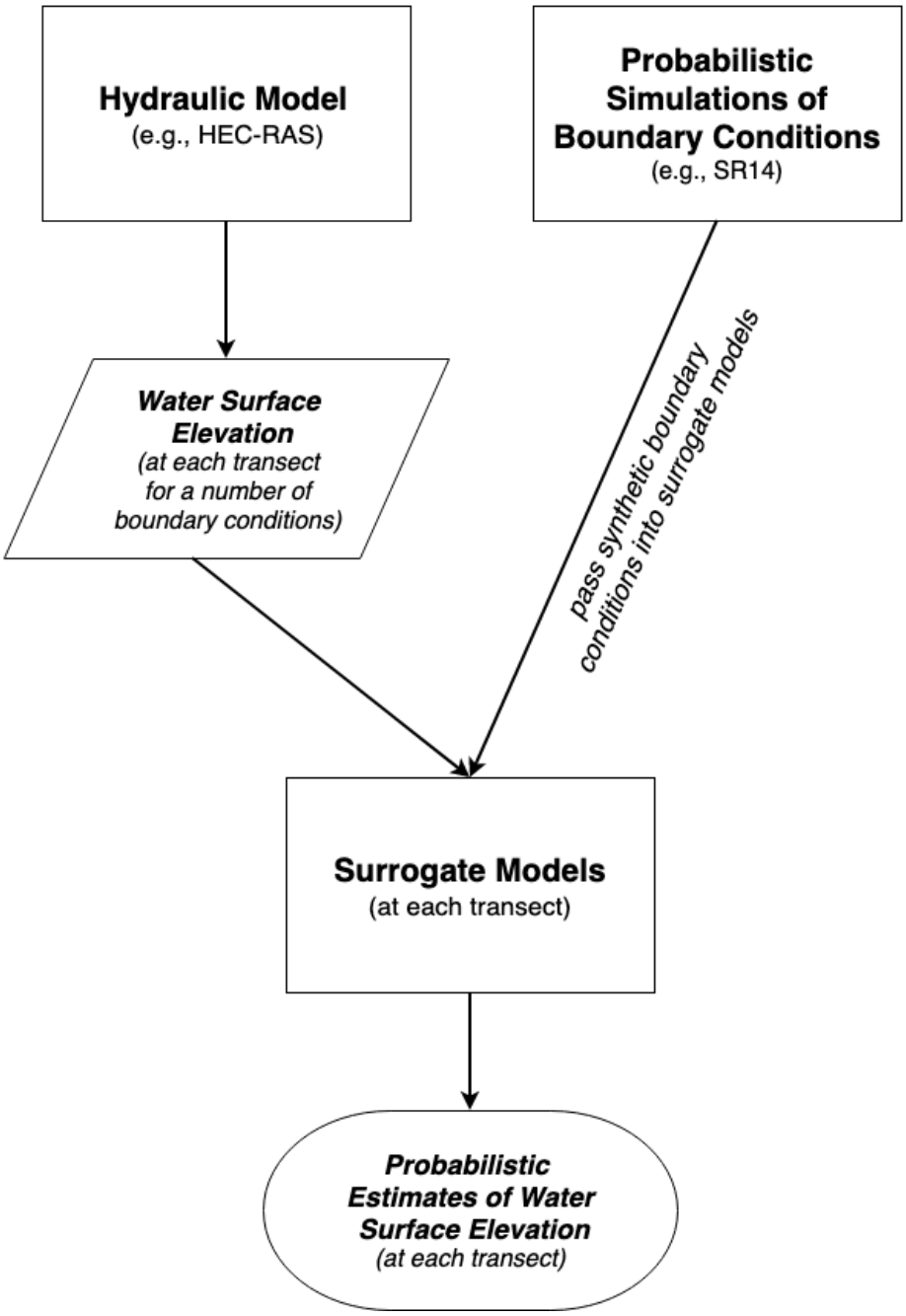

Figure 1: Schematic of hybrid statistical-physical modeling technique. Models are portrayed as squares, while circles portray model outputs.

My main methodological concern relates to the use of steady flow simulations. As the authors state themselves in the discussion, the steep catchment of the mountainous environment means a short response time for rainfall. It also calls into question the validity of using steady-state flow for the analysis. I would like the authors to explain this choice and explain what it means for the overall results? Has there been any sensitivity assessment of the results compared to an unsteady state simulation, for example?

Department of Geophysics
397 Panama Mall, Mitchell Earth Sciences Building, Stanford, CA 94305 T 650.497.6509

When originally considering merging the statistical and physical model, we started with steady flow scenarios in order to keep our simulations as simple as possible. With millions of combinations of boundary conditions, admitting discharge as a function of time would add another level of complexity to the modeling framework. However, as the reviewer mentions and as we state in the manuscript, the response time can be short, with the river rising to peak flow over 1-2 days. We completed a sensitivity assessment of steady versus unsteady simulations for a variety of hydrographs and stationary downstream boundary conditions. Figures below compare water surface elevations from the steady flow simulation of the peak discharge condition in each hydrograph to water surface elevations during the peak discharge condition from an unsteady flow simulation. Below we present results from a low, average, and extreme flow scenario (Figures 2, 4, 6, respectively).

Our results show that for many along-river locations, the steady flow approximation is reasonable. Average (standard deviation) differences between water surface elevations are 5 cm (20 cm), 7 cm (11 cm), and 40 cm (76 cm) (Figures 3, 5, 7). Large percent differences between steady and unsteady simulations are due to differences between very small numbers (e.g., Figure 7). These results show that at specific locations, unsteadiness is indeed an area of improvement, but it is currently outside the scope of what has been done. On page 22 and 23, Lines 9-10 and 1-2, we have included the following, "Thus, with co-occurring daily maximum SWL and discharge, our model may miss certain dynamics important for flooding over unsteady conditions. Furthermore, interactions between storm surge and river discharge may increase the overall elevation of the residual (Maskell et al., 2013). While beyond the scope of our present study, these unsteady characteristics are important to consider in future research."

Our methodology at this point is not intended to model any specific event perfectly, but instead to understand locations where compounding SWL and Q are statistically likely to occur together and potentially generate flooding events. This technique can also provide useful information for choosing appropriate boundary conditions for the modeling of unsteady flow scenarios. Finally, as mentioned in the manuscript, the existence of a longitudinal profile of the water surface elevation, which we were able to recreate using steady flow simulations, provided some confidence in our selection of steady flow simulations.

Department of Geophysics
397 Panama Mall, Mitchell Earth Sciences Building, Stanford, CA 94305 T 650.497.6509

Scenario 1, Low discharge
20% increase in flow, peak flow = 25cms, SWL = -1m

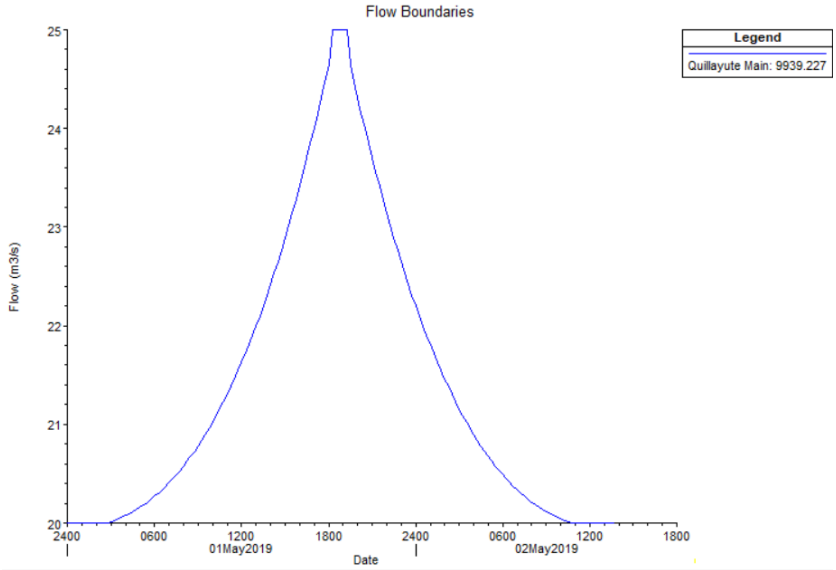

Figure 2: Hydrograph for the low discharge unsteady simulation 1. Scenario 1, Low discharge 20% increase in flow, peak flow = 25cms, SWL = -1m

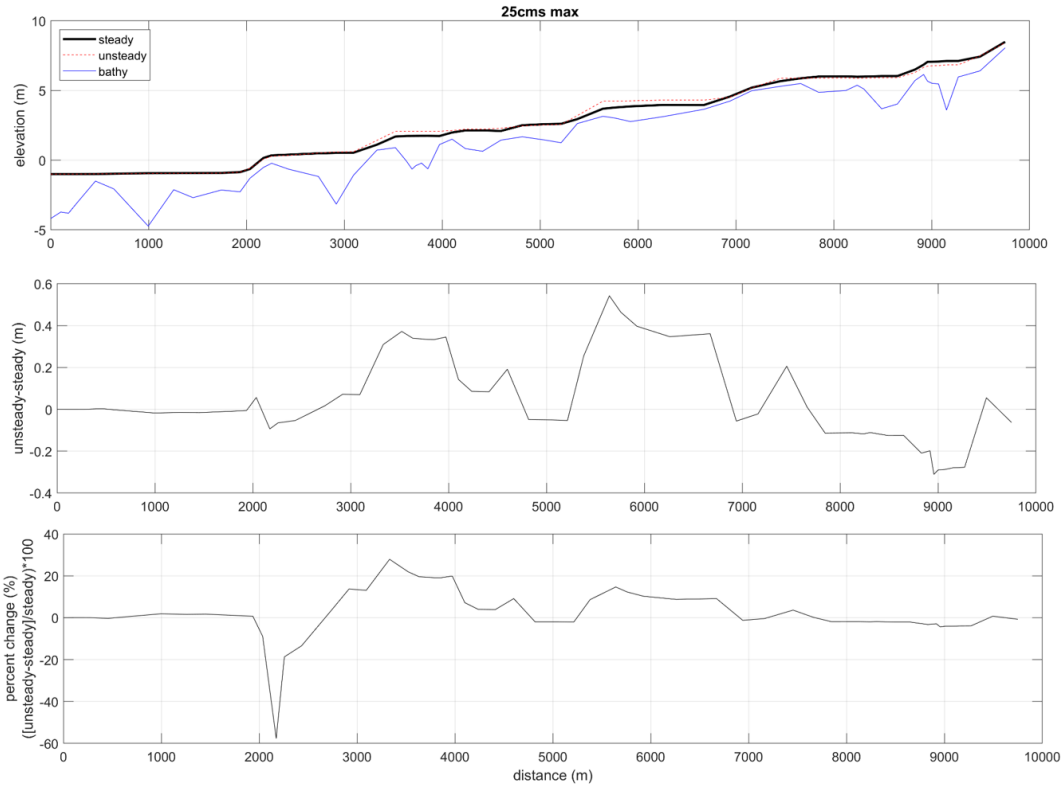

Figure 3: Comparison of the water surface elevation of the maximum discharge in a steady flow run with the water surface elevation during the maximum discharge in an unsteady flow run. Large percent change occur when dividing by small numbers.

Scenario 2, Average discharge
20% increase in flow, peak flow = 120cms, SWL = -1m

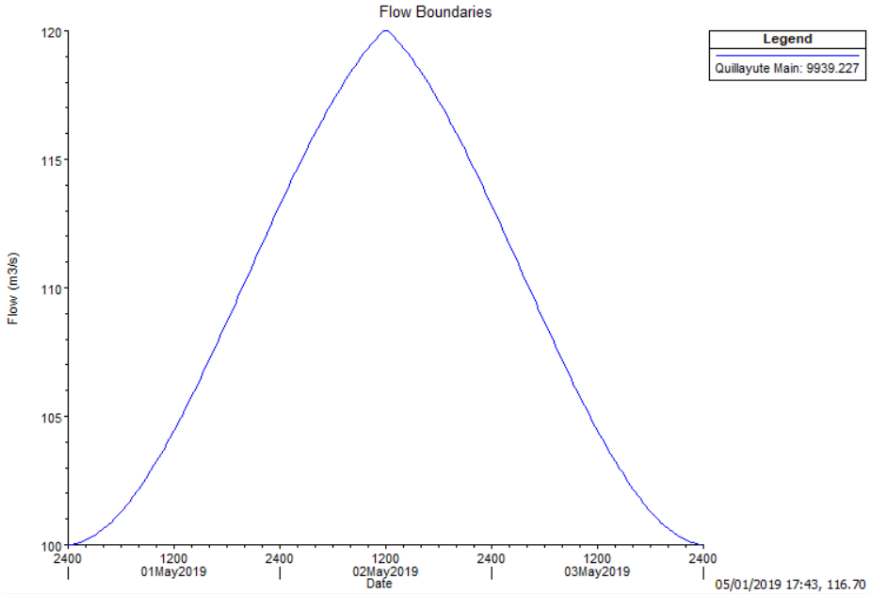

Figure 4: Hydrograph for the average discharge unsteady simulation 2.

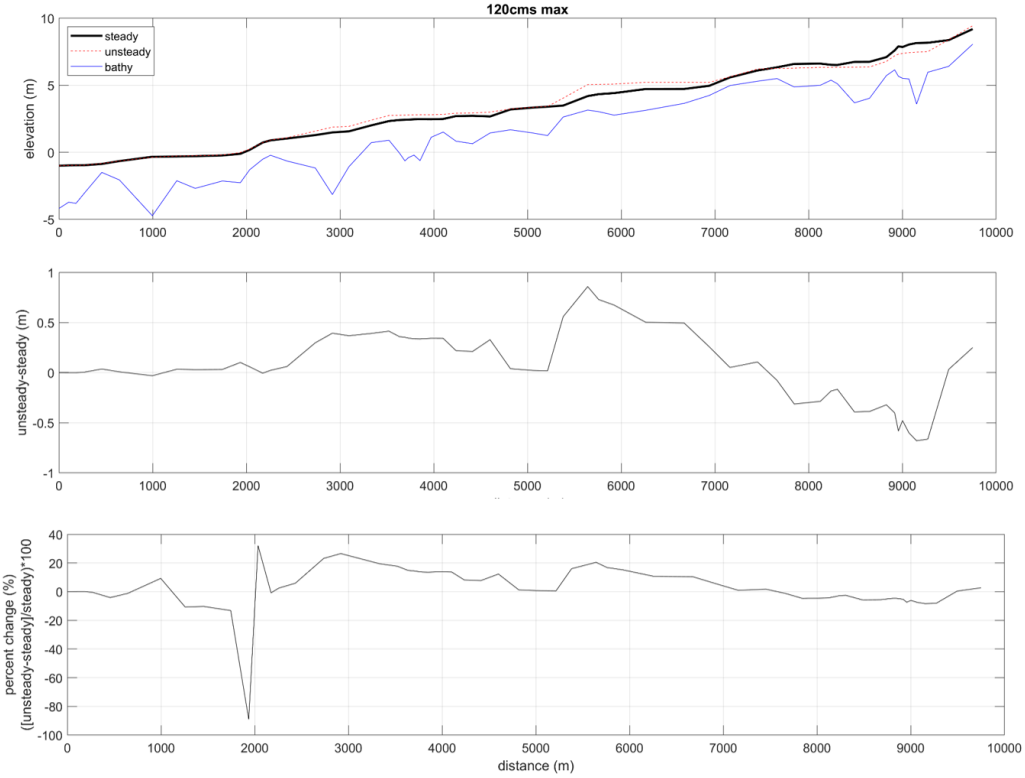

Figure 5: Comparison of the water surface elevation of the maximum discharge in a steady flow run with the water surface elevation during the maximum discharge in an unsteady flow run. Large percent change occur when dividing by small numbers

Department of Geophysics
397 Panama Mall, Mitchell Earth Sciences Building, Stanford, CA 94305 T 650.497.6509

Scenario 3, Extreme discharge

2000% increase in flow, peak flow = 884cms, SWL = -1m

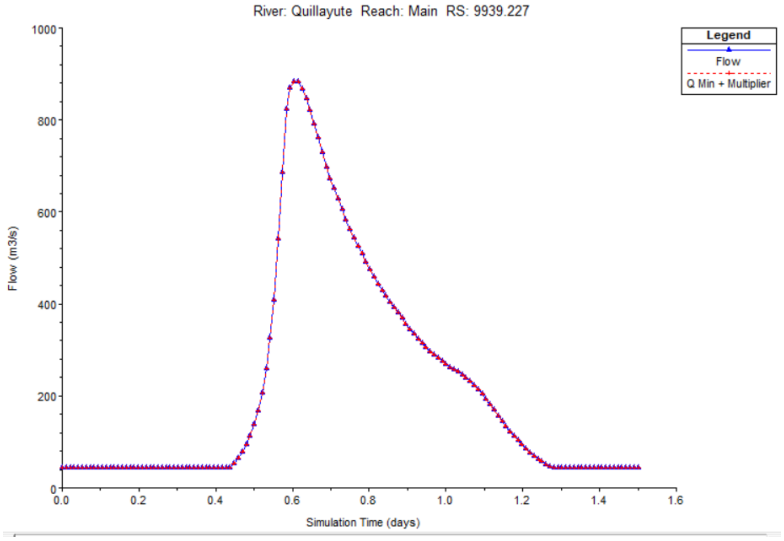

Figure 6: Hydrograph for the extreme discharge unsteady simulation 3.

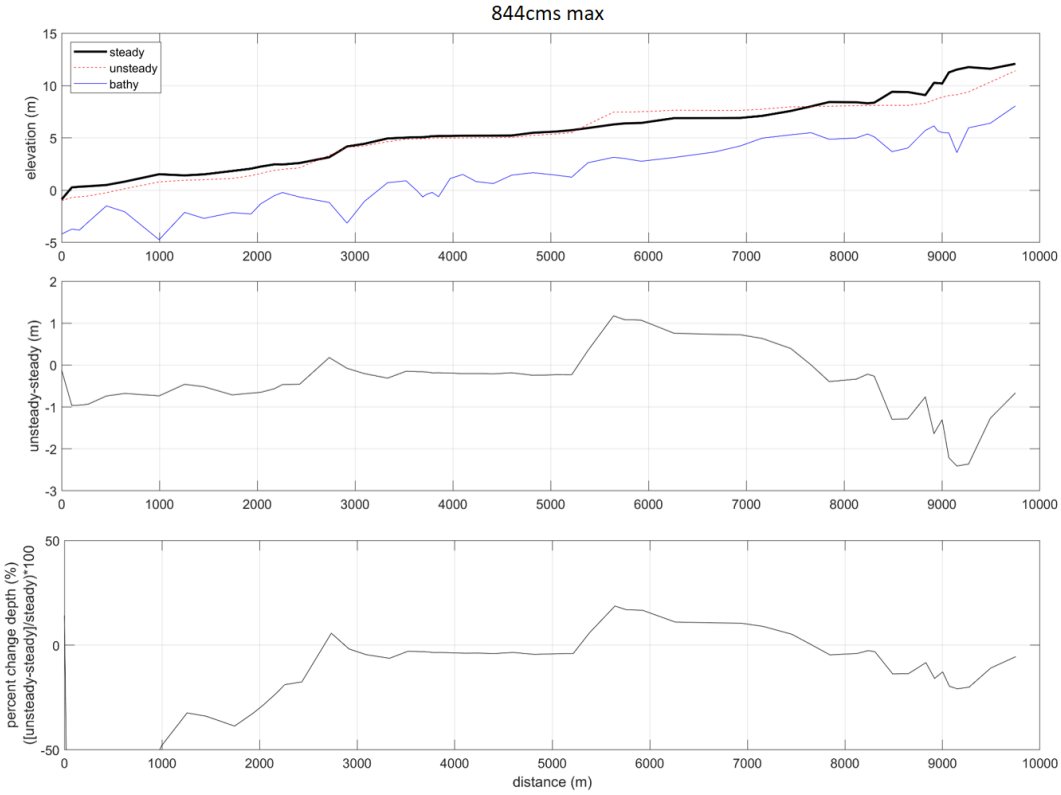

Figure 7: Comparison of the water surface profile of the maximum discharge in a steady flow run with the water surface profile during the maximum discharge in an unsteady flow run. The bottom panel is scaled to easily view values; values off the chart are up to 300% different, but for locations where the elevation goes from negative to positive.

It is not clear what Manning's coefficients are used on the floodplains. It is stated that they are estimated using 2011 Land Cover data from the Western Washington Land Cover Change Analysis project (NOAA, 2012) and visual inspection of aerial imagery. But what values were selected for different land use classes? Moreover, on page 8, line 20 the Manning coefficient of "0.005" is very low and not really representative of natural river states. Is there a specific reason for this?

The Manning's coefficients used over the floodplain ranged from 0.04 (cleared land with tree stumps) - 0.1 (heavy stands of timber/medium to dense brush). These values were extracted from Table 3-1 in Brunner, 2016. For the channel, Manning's coefficients were calibrated on a transect by transect basis to determine the best-fitting longitudinal water surface profile compared to the measured data. This technique of optimizing the Manning's coefficient is widely used in the literature when observational water surface profiles exist (e.g., Wasantha Lal, 1995 and Drisya, and Sathish Kumar, 2018). That said, due to this calibration, some of our transects are lower than what would be expected for some portions of river. However, the average of all transects is 0.025 and the majority of the transects fall between 0.02 – 0.1. We will also note that there is considerable uncertainty in the geometry of the channel. The river bathymetry was last surveyed in 2010, and in this application, merged into a DEM based on Lidar data from 2014. There are therefore other levels of uncertainty likely being absorbed into our calibration of the Manning's coefficient. To clarify this information, we have added the following text to the revised manuscript's supplemental information, Page 1, Lines 20-25 "In-channel Manning's coefficients are tuned to calibrate the model's resulting water surface elevations with that of the observed water surface data. Manning's coefficients for the rest of the computational domain (e.g., anything overbank) are estimated using 2011 Land Cover data from the Western Washington Land Cover Change Analysis project (NOAA, 2012), and visual inspection of aerial imagery and range from 0.04 (cleared land with tree stumps) - 0.1 (heavy stands of timber/medium to dense brush). These values are extracted from the HEC-RAS Hydraulic Reference Manual, Table 3-1 (Brunner, 2016)" and Page 2, Lines 15-17, "Manning's coefficients within the main channel of the Quillayute River are calibrated to best represent the water surface elevation on the day of the USGS longitudinal survey. Final Manning's coefficients range from to 0.005 to 0.1, and are on average 0.025."

How are the high water level events constructed? The possible presence of autocorrelation in the data is not mentioned – it would be good to test for this or report the results of such a test if it has been done already.

As we are not 100% clear on what the reviewer is referring to here our response will focus on how we construct high still water level events.

Still water levels (SWLs) at the downstream boundary are constructed using methods from Serafin and Ruggiero, 2014 and Serafin et al., 2017 but are also described in detail below. The motivation behind our simulations are to generate distributions of many combinations of extreme and non-extreme variables. Based on the modeling techniques used, some signals are simulated with autocorrelation, but most are not. Our focus is on representing the nonstationarities and dependencies in our bulk distributions of the simulated variables (SWLs and all its components, wave height, wave period, wave direction, climate indices, discharge) and determining how combinations of these variables may alter flooding.

SWLs from the tide gauge are first decomposed into mean sea level, tide, and non-tidal residual components. Mean sea level is determined by a linear regression applied to monthly means of the SWL record. Non-tidal residual is comprised of all water level signals not related to the astronomical tide, and is includes the intra-

annual seasonal signal, monthly mean sea level anomalies (inter-annual variability), and a high-frequency residual related to storm surge due to atmospheric pressure anomalies and wind setup. The seasonal signal is produced by a regression model that includes annual and/or semiannual harmonics, fit to the SWL time series with mean sea level removed. Monthly mean sea level anomalies are computed once the seasonal signal is removed from the water level signal by averaging each month on record. To extract storm surge after mean sea level, seasonality and monthly mean sea level anomalies have been removed, two year blocks of the water level time series are transformed into the frequency domain and, following the spectral methods of Bromirski et al., [2003], tide bands are removed and replaced with amplitude and phase estimates consistent with the concurrent nontide continuum. The result is a storm surge time series that excludes tidal and other low frequency energy. The tide was extracted from NOAA's tidal predictions and the annual (Sa) and semiannual (Ssa) harmonic constituents were removed. A SWL time series is then constructed by adding the above decomposed time series back together.

To statistically simulate daily time series of the above components

1) Storm surge is split into extreme (using a peak over threshold approach) and non-extreme components. Extreme storm surge are fit to non-stationary Generalized Pareto Distributions which include seasonality and climate indices as covariates. Non-extreme storm surge are fit to monthly logistic distributions. Storm surge is then statistically simulated using a bivariate logistic model dependent on wave height.

2) Monthly mean sea level anomalies are simulated based on a best-fit, multiple linear regression model to the Multivariate ENSO Index (MEI). Climate indices (e.g., the MEI or the Pacific/North American teleconnection pattern (PNA) which is associated with fluctuations in the jet stream) are simulated using Markov Chains to incorporate auto-correlation into the simulated signal.

3) Daily astronomical tide is simulated from a repeated deterministic tide time series such that we are simulating "modern day" extremes and not including longer term tide cycles in our analysis. The daily maximum tide is selected every day from the repeated time series. The daily maximum TWL occurs during the daily maximum tide approximately 70% of the time, therefore, for 30% of the daily data, a random estimate sampled from an exponential fit to the differences between the daily maximum TWL and the maximum daily tide.

Other suggestions

Figure 13: the grey dashed lines presumably belong to the 4 different return periods shown – it would be easier for the reader to use the same colours (but dashed) instead of grey.

Excellent suggestion, this figure has been modified.

Caption of figure 13: "the pink shaded area represents a transition zone, where neither event drives the water level". The last part is not clearly phrased. Do you mean the zone where the water level is not driven by either the coastal or river drivers alone?

Thanks for catching – the text has been changed to, "The grey shaded area represents a transition zone, where the water level is driven by a combination of SWL and Q events."

Department of Geophysics
397 Panama Mall, Mitchell Earth Sciences Building, Stanford, CA 94305 T 650.497.6509

Page 26, lines 14-15: “At low tide, a high river discharge may promote drainage of the floodwater into the ocean (Kumbier et al., 2018), increasing water levels for days at a time and prolonging exposure to flooding”. Why would a low tide that promotes drainage to the ocean lead to increased water levels? Would the opposite not lead to backwater effects?

Thanks for catching this, this statement has been removed from the text and changed to the following Page 21 - 22, Lines 11-12 and 1-2, “The outletting to the ocean as the tide recedes would artificially inflate SWLs at the tide gauge, increasing water levels for days at a time and prolonging exposure to flooding. When subtracting a tide time series from this signal, storm surge would appear to be elevated at low tide.”

In the abstract it is stated that “Understanding the relative forcing of extreme water levels along an ocean-to-river gradient will better prepare communities within inlets and estuaries for the compounding impacts of various environmental forcing”. A similar statement can be found in the conclusions. I feel that this requires more nuance. There are many steps that would be needed to make these (important) scientific insights usable by a local community for preparing themselves.

We have made this sentence less specific by writing, “Understanding the relative forcing driving extreme water levels along an ocean-to-river gradient will help communities within inlets better understand their risk to the compounding impacts of various environmental forcing, important for increasing their resilience to future flooding events.”

Page 17-line 14-15: “ADCIRC simulations confirm this phenomenon, as the river discharge peak is modeled exactly at low tide (Figure 5)”. I find it hard to see that when looking at Figure 5. Maybe help the reader a bit more? For me it seems more to be at high tide but maybe there is something I am missing.
Figure 5 (in the original manuscript) displayed only the storm surge, so lacked tide, mean sea level, seasonality, and monthly sea level anomalies. We have created a second panel within the figure (Figure 7 in the revised manuscript) which also includes tidal level from the ADCIRC simulations to help guide the reader to this conclusion.

Textual changes

Page 3, line 30. Change “. . .experiencing relative sea level rates of. . .” to “. . .experiencing relative sea level change rates of. . .” (similar comment in line 31).

This has been corrected.

Page 8, lines 10-11: add “in most cases”.

This has been corrected.

Page 8, line 30 (and the rest of the text): where is Toke Point tide gauge on Figure 1?

These labels were accidently left off our original Figure. Figure 1 in the revised manuscript now includes labels for all tide gauges, as well as a legend that reflects all mapped features.

Department of Geophysics
397 Panama Mall, Mitchell Earth Sciences Building, Stanford, CA 94305 T 650.497.6509

Page 11, line 12. Change “periosd” to “period”

This has been corrected.

Page 14, line 13. Change “subsituting" to “substituting”

This has been corrected.

Page 23, line 19: suggest to remove “regardless of the likelihood” (it is already in the return level events?)

This has been corrected.

Page 23-line 5 and 8: add “a” and “b” to Figure 13 to help the reader. References not mentioned in manuscript

This has been corrected.

Bevacqua E, Maraun D, Haff I H,WidmannM and Vrac M 2017 Multivariate statistical modelling of compound events via pair-copula constructions: analysis of floods in Ravenna (Italy) Hydrol. Earth Syst. Sci. 21 2701-2723.
Couasnon A, Sebastian A and Morales-Nápoles O 2018 A Copula-based bayesian network for modeling compound flood hazard from riverine and coastal interactions at the catchment scale: An application to the houston ship channel, Texas. Water, 10, 9, 1190
Van den Hurk B, van Meijgaard E, de Valk P, van Heeringen J and Gooijer ´ J 2015 Analysis of a compounding surge and precipitaiton event in the Netherlands Environ. Res. Lett. 10, 035001

Above suggested references have been included in the text.

Anonymous Referee #2 Received and published: 5 March 2019

The paper overall presents a good contribution, however, it needs some work Some concepts are not clear, and the reader is left ‘guessing’ about their meaning. for example, in the introduction, a reader is not aware of what ‘bivariate or multivariate processes’ are, thus they can’t understand the challenge in trying to identify them or study them.

We thank the reviewer for pointing out the lack of contextual information in the initial submission. Bivariate and multivariate processes are processes that occur from two or multiple variables, respectively. In coastal environments, multiple processes like waves, tides, storm surge, and river discharge, may combine to drive an extreme flood event. We have improved the clarity of our descriptions of multivariate and bivariate processes by removing the sentence driving confusion (Page 1, Line 21-22 original manuscript) while introducing a formal definition of a compound event in the first line of the introduction, Page 1, Lines 16-21, “Coincident

or compound events are a combination of physical processes in which the individual variables may or may not be extreme, however the result is an extreme event with a significant impact (Zscheischler et al., 2018, Bevacqua et al., 2017, Wahl et al., 2015, Leonard et al., 2014). Flooding is often caused by compound events, where multiple factors impact both open coast and estuarine environments. Storm events, for example, often generate concurrently large waves, heavy precipitation driving increased streamflow, and high storm surges, making the relative contribution of the actual drivers of extreme water levels difficult to interpret." We have also added a brief description to the abstract, Page 1, Lines 1 -2, "Extreme water levels generating flooding in estuarine and coastal environments are often driven by compound events, where many individual processes such as waves, storm surge, streamflow, and tides coincide." We hope that this revision will help readers to understand the types of events we are focused on understanding.

My major concerns are related to the method section, that currently needs much improvement. In its present state, it is much too long in some parts, and not enough clear on the overall framework, which is the added value of this work. There is far too much description of known elements, such as HEC-Ras, for example, and not enough clarity on the proposed approach. Also, it is not too clear if chapter 4 is a method or a discussion of results. As a consequence, it is very hard to understand the discussion of the results.

We agree that the amount of detail presented in the original manuscript may have added unnecessary length and detracted from the main value of the paper and point out that Reviewer 1 had a very similar comment. Therefore, in the revised manuscript, we have moved the sections describing the HEC-RAS model domain setup, validation and calibration to the Supplemental Information. We also have moved the section describing the tide gauge merging and removal of the river-influenced water levels to the Supplemental Information. Section 4 in the original manuscript was difficult to interpret, so we merged the text from this section in with methods, results, and discussion sections in the revised manuscript in a fluid way. We have also added a schematic of the hybrid-modeling framework (Figure 3, revised manuscript and below), to help to clarify and emphasize the overall framework for readers.

Department of Geophysics
397 Panama Mall, Mitchell Earth Sciences Building, Stanford, CA 94305 T 650.497.6509

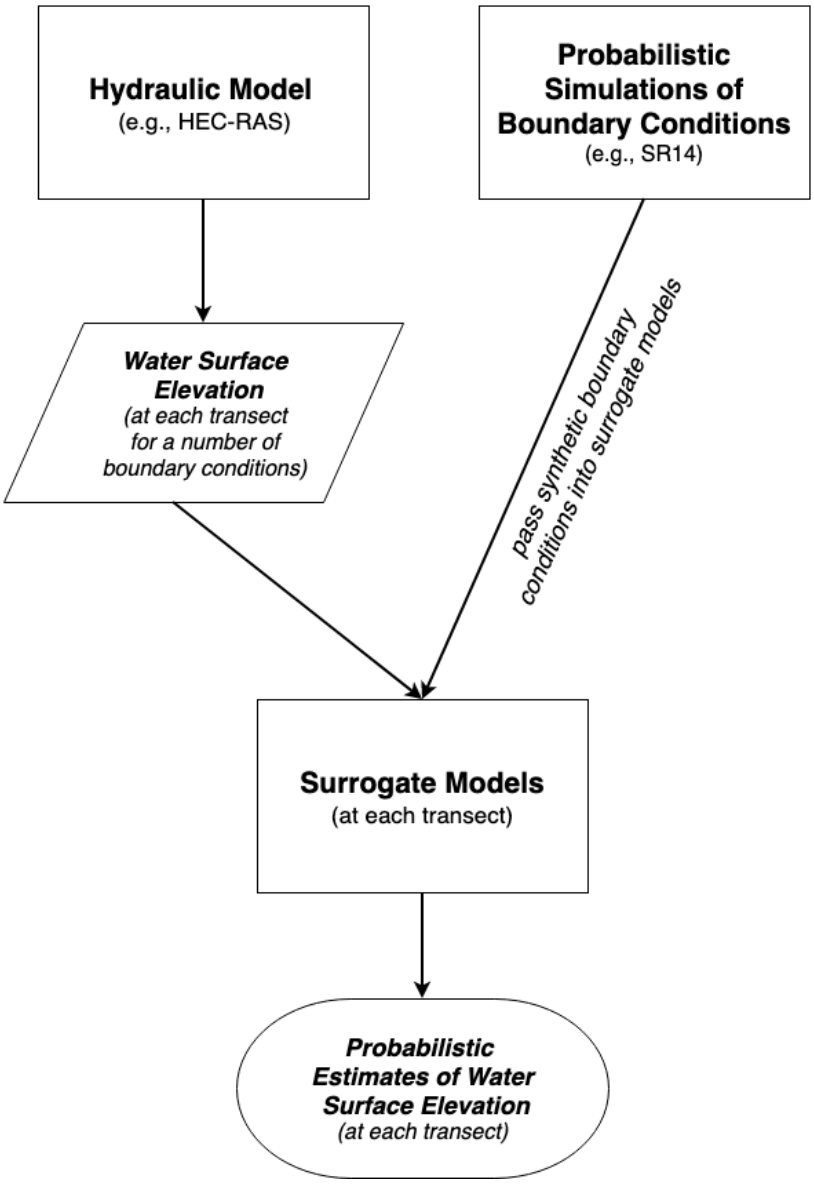

Figure 3: Schematic of hybrid physical-statistical modeling technique. Models are portrayed as squares, while circles portray model outputs.

Department of Geophysics
397 Panama Mall, Mitchell Earth Sciences Building, Stanford, CA 94305 T 650.497.6509

References:

Bevacqua, E., Maraun, D., Hobæk Haff, I., Widmann, M. and Vrac, M., 2017. Multivariate statistical modelling of compound events via pair-copula constructions: analysis of floods in Ravenna (Italy). Hydrology and Earth System Sciences, 21(6), pp.2701-2723.

Bromirski, P.D., Flick, R.E. and Cayan, D.R., 2003. Storminess variability along the California coast: 1858–2000. Journal of Climate, 16(6), pp.982-993.

Couasnon, A., Sebastian, A. and Morales-Nápoles, O., 2018. A Copula-Based Bayesian Network for Modeling Compound Flood Hazard from Riverine and Coastal Interactions at the Catchment Scale: An Application to the Houston Ship Channel, Texas. Water, 10(9), p.1190.

Drisya, J. and Sathish Kumar, D., 2018. Automated calibration of a two-dimensional overland flow model by estimating Manning's roughness coefficient using genetic algorithm. Journal of Hydroinformatics, 20(2), pp.440-456.

Leonard, M., Westra, S., Phatak, A., Lambert, M., van den Hurk, B., McInnes, K., Risbey, J., Schuster, S., Jakob, D. and Stafford-Smith, M., 2014. A compound event framework for understanding extreme impacts. Wiley Interdisciplinary Reviews: Climate Change, 5(1), pp.113-128.

Moftakhari, H., Schubert, J.E., AghaKouchak, A., Matthew, R. and Sanders, B.F., 2019. Linking Statistical and Hydrodynamic Modeling for Compound Flood Hazard Assessment in Tidal Channels and Estuaries. Advances in Water Resources.

Wahl, T., Jain, S., Bender, J., Meyers, S.D. and Luther, M.E., 2015. Increasing risk of compound flooding from storm surge and rainfall for major US cities. Nature Climate Change, 5(12), p.1093.

Wasantha Lal, A. M. "Calibration of riverbed roughness." Journal of Hydraulic Engineering 121, no. 9 (1995): 664-671.

Zscheischler, J., Westra, S., Hurk, B.J., Seneviratne, S.I., Ward, P.J., Pitman, A., AghaKouchak, A., Bresch, D.N., Leonard, M., Wahl, T. and Zhang, X., 2018. Future climate risk from compound events. Nature Climate Change, p.1.

List of Relevant Manuscript Changes:

1. *Provided formal definition of compound event*
2. *Developed new figure for modeling framework*
3. *Developed supplemental information section*
4. *Moved sections most of 3.2 and 3.2.1 to supplemental information (in original manuscript)*
5. *Removed Section 4, and moved text to results, discussion and supplemental information*
6. *Clarified Manning's Coefficient choices in text*
7. *Re-wrote sections with modeling framework for clarity*

Department of Geophysics
397 Panama Mall, Mitchell Earth Sciences Building, Stanford, CA 94305 T 650.497.6509

Department of Geophysics
397 Panama Mall, Mitchell Earth Sciences Building, Stanford, CA 94305 T 650.497.6509

What's streamflow got to do with it? A probabilistic simulation of the competing oceanographic and fluvial processes driving extreme along-river water levels

Katherine A. Serafin[1,2], Peter Ruggiero[1], Kai A. Parker[3], and David F. Hill[3]

[1]College of Earth, Ocean, and Atmospheric Sciences, Oregon State University, Corvallis, OR, USA
[2]Department of Geophysics, Stanford University, Stanford, CA, USA
[3]College of Engineering, Oregon State University, Corvallis, OR, USA

Correspondence: Katherine A. Serafin (kserafin@stanford.edu)

Abstract. Extreme water levels ~~driving~~ generating flooding in estuarine and coastal environments are often driven by compound events, ~~generated by~~ where many individual processes ~~like~~ such as waves, storm surge, streamflow, and tides coincide. Despite this, extreme water levels are typically modeled in isolated open coast or estuarine environments, potentially mischaracterizing the true risk ~~to~~ of flooding facing coastal communities. ~~We explore~~ This manuscript explores the variability of extreme water levels near the tribal community of La Push, within the Quileute Indian Reservation on the Washington state coast where a river signal is apparent in tide gauge measurements during high discharge events. To estimate the influence of ~~multivariate forcing~~ multiple forcings on high water levels ~~, we first develop a methodology for statistically simulating discharge and river-influenced water levels in the tide gauge. Next, we merge~~ a hybrid modeling framework is developed, where probabilistic simulations of joint still water level and ~~discharge occurrences~~ river discharge occurrences are merged with a hydraulic model that simulates along-river water levels. This methodology produces along-river water levels from thousands of combinations of events not necessarily captured in the observational ~~record~~records. We show that the 100-yr ~~ocean or~~ still water level event and the 100-yr ~~streamflow event does~~ discharge event do not always produce the 100-yr along-river water level. ~~Along~~ Furthermore, along specific sections of river, both still water level and ~~streamflow~~ discharge are necessary for producing the 100-yr along-river water level. Understanding the relative forcing ~~of~~ driving extreme water levels along an ocean-to-river gradient will ~~better prepare~~ help communities within inlets ~~and estuaries for~~ better understand their risk to the compounding impacts of various environmental forcing, ~~especially when~~ important for increasing their resilience to future flooding events.

1 Introduction

Coincident or compound events are a combination of ~~extreme or non-extreme forcing can result in~~ physical processes in which the individual variables may or may not be extreme, however the result is an extreme event with ~~significant impacts.~~

~~Storm events~~a significant impact (Zscheischler et al., 2018; Bevacqua et al., 2017; Wahl et al., 2015; Leonard et al., 2014). Flooding is often caused by compound events, where multiple factors impact both open coast and estuarine environments. Storm events, for example, often generate concurrently large waves, heavy precipitation driving increased streamflow, and

high storm surges, making the relative contribution of the actual drivers of extreme water levels difficult to interpret~~from tide gauge observations alone~~. Studies at the global (e.g., Ward et al. (2018)), national (e.g., Wahl et al. (2015); Svensson and Jones (2002); Zheng et al. (2013)) and regional scale (e.g., Odigie and Warrick (2017); Moftakhari et al. (2017)) have evaluated the likelihood for variables such as high river flow and precipitation to occur during high coastal water levels, demonstrating that ~~relationships~~ dependencies often exist between these individual processes. ~~Understanding the nature of the dependency between bivariate or multivariate processes is one of the first steps in piecing together the contributors to flooding events.~~

Around river mouths, the elevation of the water level measured by tide gauges, or the still water level (SWL), varies depending on the mean sea level, tidal stage, and the non-tidal residual contributors which may include the following forcings; storm surge, seasonally-induced thermal expansion (Tsimplis and Woodworth, 1994), the geostrophic effects of currents (Chelton and Enfield, 1986), wave setup (Sweet et al., 2015; Vetter et al., 2010), and river discharge. Most commonly, estimates of non-tidal residuals are determined by subtracting predicted tides from the measured water levels. However, residuals computed in this way often contain artifacts of the subtraction process from phase shifts in the tidal signal and/or timing errors (Horsburgh and Wilson, 2007). Another approach ~~to describing~~ for extracting the non-tidal residual is through the skew surge, which is the absolute difference between the maximum observed water level and the predicted tidal high water (de Vries et al., 1995; Williams et al., 2016; Mawdsley and Haigh, 2016). While this methodology removes the influence of tide-surge interaction from the non-tidal residual magnitude, it does not differentiate between the many factors contributing to the water level, an important step for distinguishing when and why high water~~(~~, and thus flooding~~)~~ , is likely to occur.

Hydrodynamic and hydraulic models have recently been used in attempts to quantify the relative importance of river and ocean-forced water levels to flooding. The nonlinear coupling of wind and pressure driven storm surge, tides, wave-driven setup, and riverine flows has been found to be a vital contributor to overall water level elevation (Bunya et al., 2010). Furthermore, river discharge is often found to interact nonlinearly with storm surge (Bilskie and Hagen, 2018), exacerbating the impacts of coastal flooding (Olbert et al., 2017), which suggests that the extent or magnitude of flooding is often underpredicted when both river and oceanic processes are not modeled (Bilskie and Hagen, 2018; Kumbier et al., 2018; Chen and Liu, 2014). The computational demand of two and three-dimensional hydrodynamic models, however, typically precludes a large amount of events to be examined. Therefore, while accurately modeling the physics of the combined forcings, researchers taking this approach are often limited to modeling only a ~~few select cases.~~ select number of boundary conditions. On the other hand, statistical models allow for the investigation of compound water levels through the simulation of combinations of dependent events which may not have been physically realized in observational records (Bevacqua et al., 2017; van den Hurk et al., 2015) . In addition, researchers have recently begun to generate hybrid models that link statistical and physical modeling approaches for understanding compound flood events (Moftakhari et al., 2019; Couasnon et al., 2018). Similar to the results solely from hydrodynamic and hydraulic models, statistical and hybrid modeling strategies show that simplifications of the dependence between multiple forcings may lead to an underestimation of flood risk.

This study explores the influence of oceanographic and ~~fluvial processes driving~~ riverine processes on extreme water levels along a coastal river where there is a substantial ~~fluvial~~ river signal recorded in the tide gauge. ~~Our study site, the Quillayute River, terminates in the Pacific Ocean at La Push, Washington, an incorporated tribal community within the Quileute Indian~~

~~Reservation.~~ In order to better understand the river- and ocean-forced water levels at this location, a hybrid methodology is developed for ~~defining and removing~~ linking statistical simulations of ocean and river boundary conditions with a hydraulic model that simulates along-river water levels. First, river-influenced water levels ~~from SWLs measured at tide gauges. Both~~ are defined and removed from SWLs. Then, both river discharge and river-influenced water levels are ~~then~~ incorporated into a non-stationary, probabilistic total water level model~~. This~~ , which allows for multiple synthetic representations of joint ocean and ~~fluvial~~ riverine processes that may not have occurred in the relatively short observational records. Next, a 1-dimensional hydraulic model is used to simulate water surface elevations along a 10 km stretch of river. Surrogate models are generated from the hydraulic model simulations and used to extract along-river water levels for each probabilistic joint-occurrence of SWL and river discharge ~~. Finally,~~ in a computational efficient manner. Rather than determining the along-river return level from an equivalent return level forcing (e.g., the 100-yr discharge event drives the 100-yr water level), spatially-varying ~~extreme event~~ along-river return levels are ~~derived and discussed.~~ extracted and matched to the driving boundary conditions. This technique allows for a spatially explicit analysis of the ocean and river conditions generating extreme water levels.

The following sections describe the study area, present the hybrid modeling framework linking oceanographic and ~~fluvial~~ riverine systems, and evaluate the compounding drivers of along-river extreme water levels~~along this river system~~.

2 Study Area

The Quillayute River is located in Washington state along the US West coast and drains approximately 1630 km^2 of the northwestern Olympic Peninsula into the Pacific Ocean (Czuba et al., 2010). The Quillayute River is approximately 10 km long, is formed by the confluence of the Bogachiel and Sol Duc Rivers (Figure 1), and enters the Pacific Ocean at La Push, Washington, home to the Quileute Tribe. The Quileute Indian Reservation is approximately 4 km^2 and the majority of community infrastructure sits at the river mouth, bordering the river and open coast. The Quileute Harbor Marina is also situated just inside the river mouth, and is the only port between Neah Bay and Westport, Washington. Rialto spit, which connects Rialto Beach to Little James Island, contains a rocky revetment which protects the marina and the community from ocean and storm wave impact.

The Quillayute River is a natural, unstablized river that is relatively straight at the confluence of the Bogachiel and Sol Duc rivers and increases in sinuosity moving towards the river mouth. Channel-bed materials are coarse (gravel and cobble) in the free-flowing channels and dominated by sand in the small estuary (Czuba et al., 2010). Upstream of river km 3 there are numerous point bars and bends in the river. Between river km 1.5 and 3, the Quillayute is braided with several side channels, usually containing woody debris (Czuba et al., 2010). The channel is straight near the river mouth and is confined by the Rialto spit revetment before draining into the Pacific Ocean.

The oceanic climate of the coastal Pacific Northwest (PNW) is cool and wet with a small range in temperature variation and the majority of rainfall between October and May. Four river basins, the Sol Duc, Bogachiel, Calawah, and Dickey rivers, feed into the Quillayute River and comprise the majority of the watershed. Streamflow in the region is primarily from storm-derived rainfall in the winter and snowmelt during the spring and summer (WRCC, 2017).

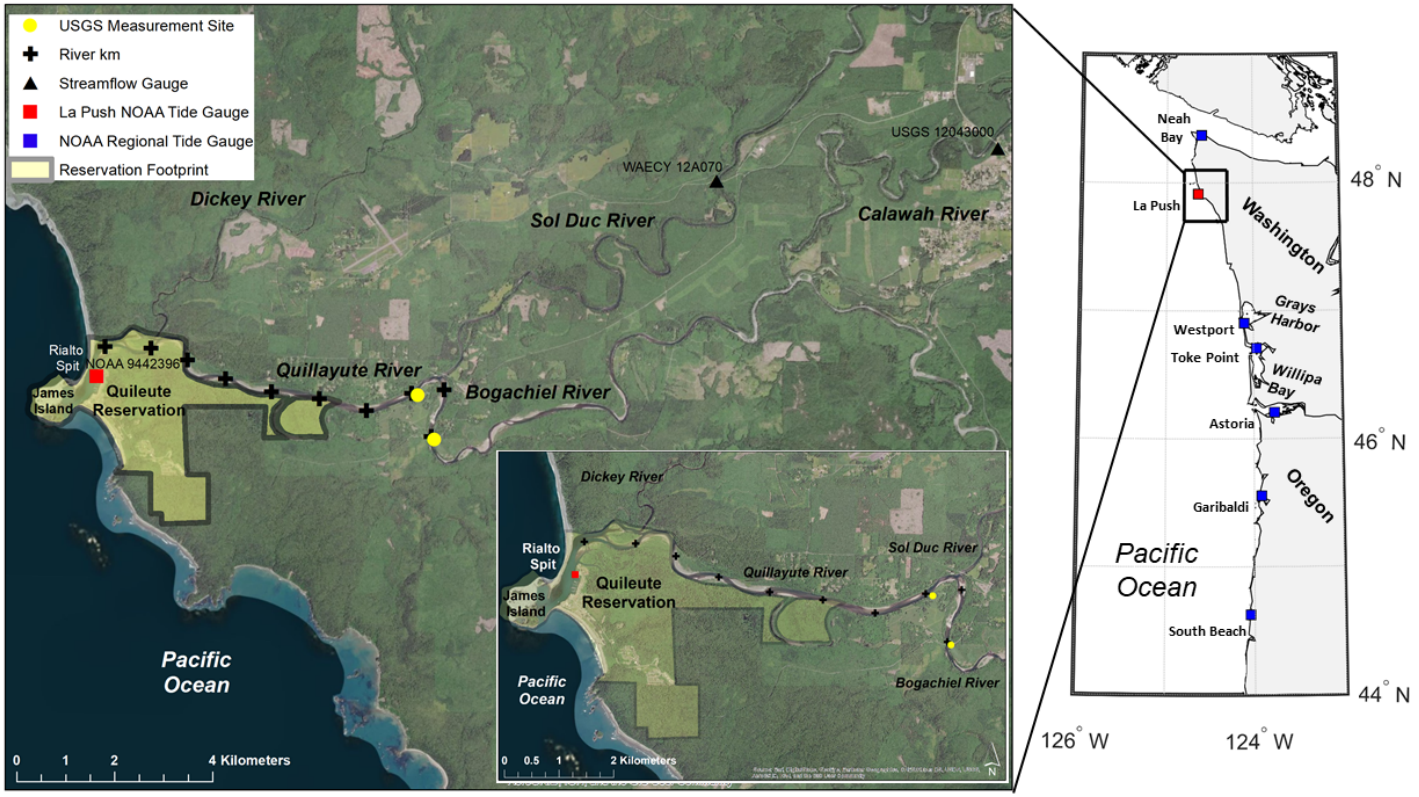

Figure 1. Map of study area (left), which is denoted on the regional map (right) in the black box. The La Push tide gauge is represented as a red square while other regional tide gauges are represented as blue squares. The Calawah and Sol Duc river gauges are represented as black triangles and USGS measurement sites from the May 2010 survey (see supplemental information) are ~~depcited~~ depicted as yellow circles. Approximate river kilometers are denoted as black crosses on the study area map.

Oceanographically-driven SWLs are generally comprised of ~~non-tidal residuals, astronomical~~ mean sea level, tides, and ~~mean sea level~~non-tidal residuals, which include storm surge. Regional variations in shelf bathymetry, shoreline orientation, storm tracks (Graham and Diaz, 2001), seasonality (Komar et al., 2011), and winds drive differences in storm surge along the US West coast. However, the US West coast's narrow continental shelf, in relation to broad-shelved systems, controls the magnitude of storm surge, ~~and it~~ whcih is rarely larger than 1 m (Bromirski et al., 2017; Allan et al., 2011). The PNW is also influenced by a unique interannual climate variability due to the El Niño Southern Oscillation. During El Niño years, the PNW experiences increased water levels for months at a time, along with changes in the frequency and intensity of storm systems (Komar et al., 2011; Allan and Komar, 2002). In the PNW, tides are micro- and mesotidal, and at La Push the tidal range is mixed, predominantly semidiurnal, with a mean range of 1.95 m and a great diurnal range of 2.58 m (https://tidesandcurrents.noaa.gov/datums.html?id=9442396).

Global rise in sea level and local changes in vertical land motions result in significant longshore variations of relative sea level along the Washington coastline. The northern Washington coast is experiencing relative sea level rates of -1.85 $\pm$ 0.42 mm/yr due to a rising coastline, while relative sea level in Willapa Bay in southern Washington is 0.94 $\pm$ 2.14 mm/yr (Komar et al., 2011). Tide gauge records at La Push are too short to calculate robust trends in sea level, however, sea level is likely rising in this location, rather than falling, partly due to local land subsidence (Miller et al., 2018).

~~Digital Elevation Model (DEM) used for the HEC-RAS simulations of the Quillayute River. HEC-RAS cross sections are depicted as grey lines. Approximate river kilometer and the location of the tide gauge are depicted as diamonds and a square, respectively.~~

3 Data

4 ~~Data and methods~~

3.1 ~~Modeling framework~~

~~Return level, or design, events are typically assessed via analyses of available observational datasets. However, observational records rarely extend more than a few decades, suggesting that all combinations of jointly-occurring processes generating extreme water levels may not have been physically realized. Therefore, in order to understand the oceanographic and fluvial drivers of extreme water levels along the Quillayute River from a full range of possible forcing conditions, we develop a methodology to merge statistically simulated joint SWL and discharge records with a one-dimensional (1D) hydraulic river flow model. This approach is designed to allow for an interpretation of extreme water levels as if different physically plausible combinations of individual driving processes had been available to be sampled over the last thirty years.~~

~~First, a method is developed to define and model river-influence in the SWLs. Next, combinations of daily maximum SWL and river discharge are statistically simulated to create many random realizations of joint SWL-discharge forcing using the Serafin and Ruggiero (2014) full simulation total water level model. Care is taken to appropriately model both the non-stationarity of each signal, as well as the dependence between the signals. A range of SWL-discharge conditions are modeled using the US~~

Army Corps of Engineers' (USACE) Hydrologic Engineering Center's River Analysis System (HEC-RAS; Brunner (2016)) to produce surrogate models for generating along-river water levels. The surrogate models are then used to produce water levels at a series of transects for each statistically simulated SWL-discharge event. The synthetic SWL-discharge simulations paired with HEC-RAS water surface profiles allows for an analysis of the dominant drivers of extreme water levels along the river. Descriptions of the hydrodynamic and statistical models, as well as the overall framework for modeling spatially-varying water levels are described in the following sections.

3.1 Hydraulic model domain and setup

HEC-RAS is a model that is used to estimate water surface elevations in rivers and streams in both steady and unsteady flow and under subcritical, supercritical, and mixed flow regimes (Goodell, 2014). HEC-RAS has been previously used to model water surfaces for a range of applications including, but not limited to, floodplain mapping (Yang et al., 2006), flood forecasting (Saleh et al., 2017), dam breaching (Butt et al., 2013), and flood inundation (Horritt and Bates, 2002). HEC-RAS computes water levels by solving the 1D energy equation with an iterative procedure, termed the step method, from one cross-section to the next (Brunner, 2016). For subcritical flows, the step procedure is carried out moving upstream; computations begin at the downstream boundary of the river and the water surface elevation at an upstream cross-section is iteratively estimated until a balanced water surface is obtained. Energy losses between cross-sections are comprised of a frictional loss via the Manning's Equation and a contraction/expansion loss via a coefficient multiplied by the change in velocity head (see Brunner (2016) for more details).

In this application, HEC-RAS is used to model 1D water levels under gradually varied, steady flow conditions at specified transects along the Quillayute River. While a simplification of flood processes, this methodology is commonly used to create flood hazard maps. HEC-RAS model runs require detailed terrain information for the river network, including bathymetry and topography for the floodplains of interest. Topography data is sourced from a 2014 U.S Army Corps of Engineers (USACE) lidar survey (**?**). Bathymetry data is developed by blending two NOAA digital elevation models (DEM): National Geophysical Data Center's (NGDC) La Push, WA tsunami DEM (1/3 arc second; **?**) and the coastal relief model (3 arc seconds; **?**). These datasets, however, do not accurately resolve the channel depths of the Quillayute River inland of the coast, so a 2010 US Geological Survey (USGS)-conducted bathymetric survey of the river is also blended into the DEM (Czuba et al., 2010).

In 2010, depths of along-river cross sections and an 11 km long longitudinal profile from the Bogachiel River (Figure 1) to the mouth of the Quillayute River were surveyed (Czuba et al., 2010). The survey of the longitudinal river profile also recorded the elevation of the water surface. Ideally, the collected bathymetry dataset would be merged directly into the existing DEM. The Quillayute River, however, is uncontrolled and meanders over time, producing a variation in the location of the main river channel between the DEM and the high-resolution USGS-collected bathymetric data. Therefore, the USGS bathymetric profiles are adjusted to match the location of the DEM channel. While a product of multiple datasets and processing steps, the final DEM provides bathymetric/topographic data with the most up-to-date channel depths for the Quillayute River (Figure 6).

A series of 58 transects are extracted from the DEM using HEC-GeoRas (?) and written into a geometric data file for input into HEC-RAS (Figure 6). Each river transect extends across the floodplain to the 10 m contour, where applicable. Otherwise, each transect terminates at the highest point landward of the river. Because HEC-RAS computes energy loss at each transect via a frictional loss based on the Manning's equation, Manning's coefficients, an empirically derived coefficient representing resistance of flow through roughness and river sinuosity, are selected for the river channel and the floodbanks. In-channel Manning's coefficients are tuned to calibrate the model's resulting water surface elevations with that of the observed water surface data (see section 3.2.1). Manning's coefficients for the rest of the computational domain (e.g., anything overbank) are estimated using 2011 Land Cover data from the Western Washington Land Cover Change Analysis project (?) and visual inspection of aerial imagery. Model domain boundary conditions are chosen as the water surface elevation at the tide gauge (m; downstream boundary) and river discharge from a combination of records representing the Quillayute River watershed ($m^3 s^{-1}$; upstream boundary).

3.0.1 HEC-RAS model validation

Observational records in the region are generally sparse; one tide gauge exists in the marina near the river mouth and hourly discharge measurements are only located on only two of the four rivers which feed into the Quillayute watershed are gauged (Figure 1). The closest gauge is located 7 miles upriver from the Quillayute River on the Sol Duc River gauge (WA Dept of Ecology 12A070) and measures approximately 9 years (2005-2014) of is located 7 miles upriver from the Quillayute River and measures hourly discharge and stage observations from 2005-2014. The second river gauge is located on the Calawah River (USGS 12043000), which approximately 15 miles upriver from the Quillayute River. The Calawah River flows into the Bogachiel River, and has hourly discharge and stage measurements from 1989 - 2016. While the Calawah River gauge is located approximately 15 miles upriver from the Quillayute River, the steep catchment drives a short response time in rainfall and the record is highly correlated with the The hourly record of discharge measurements from the Sol Duc River gauge.

In order to determine the dominant inputs to Quillayute River discharge, combined estimates of the Sol Duc and Calawah Rivers are compared to measurements taken on the Quillayute River in May 2010 (see Figure 1 for measurement location; Czuba et al. (2010)). Combined discharge estimates from the Sol Duc and Calawah rivers underpredict streamflow in the Quillayute River by approximately 33% is 100% complete, while the Calawah River is 99% complete. An area scaling watershed analysis (Gianfagna et al., 2015) is undertaken to rectify the discharge by the amount of ungauged watershed. The watershed delineation shows that the Bogachiel, Calawah, Sol Duc, and Dickey rivers account for 24%, 22%, 37%, and 17% of the total Quillayute River watershed area, respectively. Noting the similar watershed characteristics and proportional areawatershed areas, the contribution of the Bogachiel River is estimated by scaling the Calawah River discharge measurements by a factor of 2.09. Combined discharge estimates from the Sol Duc River and Bogachiel River, computed using the above scaling factor , are also compared to the Quillayute discharge This scaling factor for estimating Bogachiel River discharge is validated by comparing to 8 discharge point measurements taken during the 2010 survey.Using this methodology, the discharge estimates of the Quillayute River fall within the uncertainty of the discrete USGS measurements (Table ??).

~~Quillayute River discharge measurements from the USGS survey (Czuba et al., 2010) compared to the Quillayute River discharge estimates computed by adding the Sol Duc USGS gauge measurements with the Bogachiel River discharge, estimated via scaling of the Calawah River gauge measurements. The parenthesis in the last column is the standard deviation of USGS survey measurements (m^3s^{-1}). Date of Survey Sol Duc (m^3s^{-1}) Calawah (m^3s^{-1}) Bogachiel (m^3s^{-1}) Quillayute (m^3s^{-1}) Quillayute (m^3s^{-1}) (estimated)(estimated) (measured)4/20/2010 52 28 58 110 116 (7)4/21/2010a 48 25 53 101 108~~ a U.S. Geological Survey ~~(1) 4/21/2010b 48 25 52 100 103 (3) 4/21/2010c 46 24 50 96 107 (1) 5/4/2010a 73 69 144 217220 (5) 5/4/2010b 70 66 137 207 207 (4) 5/5/~~USGS) survey in 2010 ~~59 51 107 166 170 (3) 5/6/2010 50 40 84 134 136 (3)~~

~~a) Bathymetry and longitudinal profile from the Bogachiel River to the mouth of the Quillayute River surveyed by the USGS in May of 2010 (black). The longitudinal water level for the calibrated HEC-RAS model is depicted in blue. b) Percent difference between the measured (black) and HEC-RAS modeled (blue) water level. c) Actual difference between the measured (black) and HEC-RAS modeled (blue) water level.~~

~~The longitudinal measured water surface profile allows for the verification and calibration of HEC-RAS modeled water surface elevations on the day of the survey (Figure **??**). HEC-RAS is run using discharge of the watershed-scaled Bogachiel River as the upstream boundary condition during the hour of the field survey and this discharge is combined with a lateral inflow~~ see supplemental information). Discharge for the Quillayute River is estimated by adding together discharge from the Sol Duc ~~River around river km 8.5. Manning's coefficients along the Quillayute are calibrated to best represent the water surface elevation on the day of the survey. The final calibrated HEC-RAS model produces a water surface elevation with an average bias less than 1% (less than 1 cm) and an average standard deviation of approximately 5% (7.5 cm). The maximum difference between the two water surfaces is approximately 14 cm (20%). The percent difference between the depth of the observed and modeled water surface is almost always less than 10% (Figure **??**). Final Manning's coefficients range from to 0.005 to 0.1, and are on average 0.025.~~ and Boagachiel rivers.

3.1 ~~Total water level simulation model~~

Hourly measured SWLs ~~and predicted tide measurements~~ at the La Push tide gauge (NOAA station 9442396, 2004 - 2016) relative to Mean Lower Low Water (MLLW) are downloaded, transformed into NAVD88~~to match the DEM~~, and decomposed into mean sea level (η_{MSL}), tide (η_A), and non-tidal residual (η_{NTR}). The η_{NTR} is further decomposed into monthly mean sea level anomalies (η_{MMSLA}), seasonality (η_{SE}), and storm surge (η_{SS}), using methods described in Serafin et al. (2017). ~~A 6th geophysical signal recorded by the tide gauge, the river-influenced water level (η_{R_i}) , is also evaluated and removed from the Peak η_{SS} signal (see section 4.2 for description and methods)~~events at La Push are found to be the highest on record compared to all US West coast tide gauge stations (Serafin et al., 2017). Upon further investigation of the η_{SS} record, a large portion of extreme η_{SS} events occur during low wave events (Figure 2a) and high river discharge events (Figure 2b). This is inconsistent with η_{SS} in Westport, Washington (Figure 2a and Figure 2c), just south of La Push, and with other tide gauges along the US West coast (not shown). It is therefore hypothesized that the anomalously large signal seen in the η_{SS} is river-induced.

~~The continuous~~

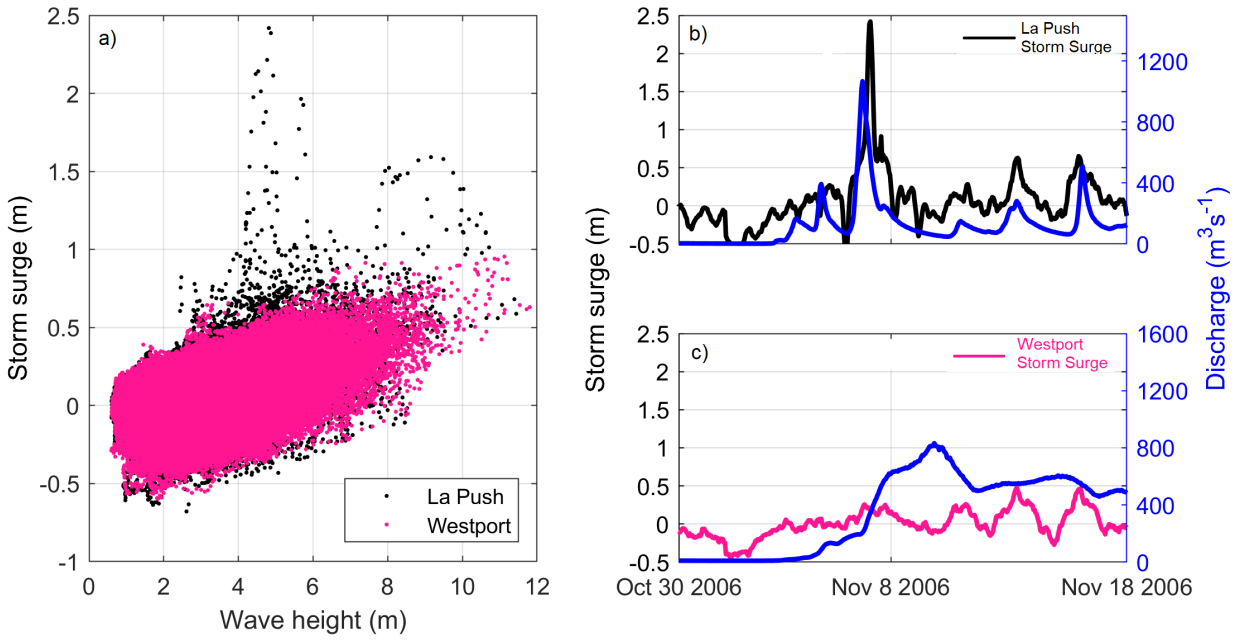

Figure 2. a) The joint relationship between storm surge and wave height for La Push, Washington (black) and Westport, Washington (pink). Example storm surge and discharge relationship at b) La Push and c) Westport, Washington.

To further investigate the anomalously large η_{SS} at the La Push tide gauge~~record begins in 2004, recording 12 years of water levels . This record , however, does not capture the extreme water levels occurring during the 1982/83 and 1997/98 El Niños. Therefore,~~ the hydrodynamic model ADvanced CIRCculation (ADCIRC, Luettich Jr et al. (1992)) and Simulating Waves nearshore (SWAN, Zijlema (2010)) model (ADCSWAN; Dietrich et al. (2011)) is used to simulate water levels at the tide gauge during a storm event corresponding with the peak river discharge on record occurring on January 8, 2009. ADCIRC is run in 2D depth-integrated barotropic mode which performs well for calculating water surface elevations during storm events (Weaver and Luettich, 2010). SWAN is run in non-stationary mode on an unstructured grid, allowing for tight coupling to ADCIRC. The model is run with two forcing implementations: one including a full forcing of waves, wind, pressure, streamflow, sea level anomalies, seasonality, and tides and one including only streamflow and tides. Once the river-influenced water level is validated, it is removed from the η_{SS} signal and saved as a 6th geophysical variable (η_{Ri}, see supplemental information for removal technique).

Because of the short length of the La Push tide gauge record, decomposed water levels from the La Push tide gauge are merged with decomposed water levels from the Toke Point tide gauge (~~beginning in 1980,~~ NOAA station 9440910) to create a combined water level record ~~representing a larger range of extreme conditions. η_A and η_{SE}, water level components deterministic to the La Push tide gauge, are extended to 1980. Water level components influenced by regional or local forcings like η_{MMSLA} and η_{SS}, are compared before combining. η_{MMSLA} between the Toke Point and La Push tide gauges are~~

similar, so Toke Point η_{MMSLA} are appended to the beginning of the La Push η_{MMSLA}. Toke Point, however, has slightly higher magnitude η_{SS} than La Push and there is a noticeable offset in the highest η_{SS} peaks. A correction is thus applied to the Toke Point η_{SS} before appending it to the beginning of the La Push η_{SS}. η_{MSL} is extended back to 1980 using relative sea level rise trends for the region. with a length of 36 years. Details of this methodology are explained in the corresponding supplemental information, as well as in Serafin et al. (2019). Once the two tide gauges are merged, the combined hourly tide gauge record extends from 1980 - 2016 and is 97% complete. Discharge measurements sampled at 15 minute intervals for the Calawah and Sol Duc rivers are interpolated to hourly increments to match the timing of the SWL measurements. At the hourly scale, the Calawah River record is 99% complete, while the Sol Duc River record is 100% complete.

4 Methods

Return level flood magnitudes, such as the 100-yr event, are typically assumed to be driven by a specific forcing event, such as the 100-yr rainfall or storm surge. However, for processes driven by multiple dimensions, different sizes and combinations of forcing conditions could potentially generate extreme flood magnitudes. To explore the role of compounding forcings in generating extreme water levels, a hybrid modeling framework is developed by merging a hydraulic model simulating river flow with probabilistic simulations of jointly occurring boundary conditions, in this case SWL and river discharge (Figure 3). Statistical simulations allow for long, synthetic records of joint forcings that may not have occurred in the short observational records but are physically capable of co-occurring. Modeling all of the statistically simulated boundary conditions in a hydraulic model to output along-river water levels would be prohibitively expensive. As an alternative to time consuming simulations, surrogate models (Razavi et al., 2012) are developed to approximate the response of a hydraulic model simulation at each along-river location. This technique allows for the analysis of along-river water levels driven by a variety of boundary conditions. Long synthetic records on the order of 500 years allows for the direct empirical extraction of water level return levels rather than an extrapolation from historic observational forcing conditions. In addition, the large sample space of simulated variables permits a comparison of event-based return levels, where the 100-yr water level is determined by the 100-yr forcing, to response-based return levels, where the 100-yr water level is derived and then mapped to its respective forcing conditions. This novel framework is flexible for input of any statistical or hydraulic model. In this application, we use the Serafin and Ruggiero (2014) full simulation total water level model and the US Army Corps of Engineers' (USACE) Hydrologic Engineering Center's River Analysis System (HEC-RAS; Brunner (2016)), which are described in more detail below.

4.1 Probabilistic simulations of boundary conditions

The non-stationary, probabilistic full simulation model of Serafin and Ruggiero (2014) (hereinafter , SR14) was developed to produce synthetic time series of daily maximum total water levels (TWLs), the combination of waves, tides, and non-tidal residuals, on open-coast sandy beaches. SR14 simulates the individual components of the TWL in a Monte Carlo sense, while appropriately accounting for any dependencies existing between the variables. This modeling technique is able to include

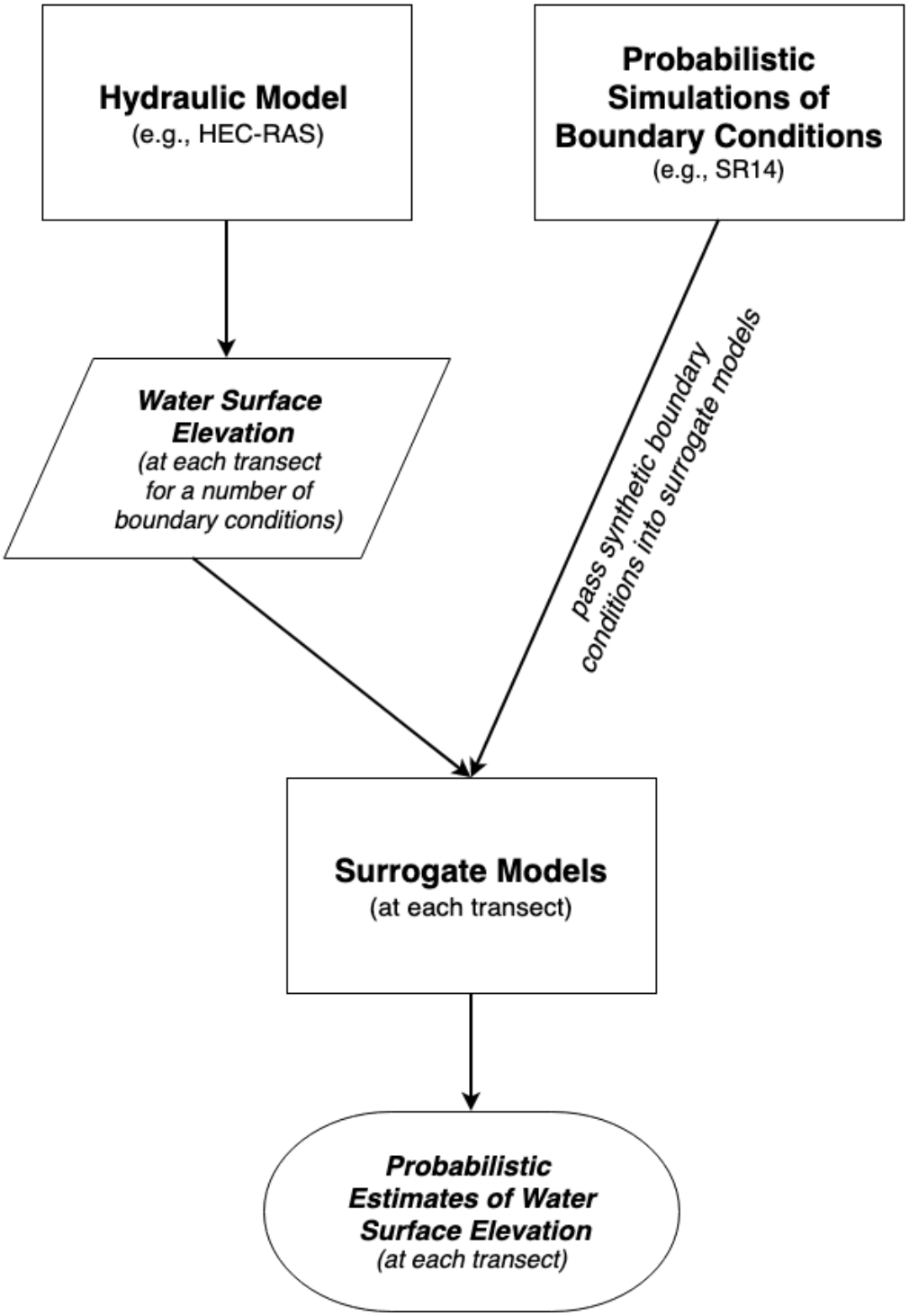

Figure 3. Schematic of hybrid statistical-physical modeling technique. Models are portrayed as squares, while circles portray model outputs.

non-stationary processes influencing extreme and non-extreme events, such as seasonality, climate variability, and trends in wave heights and water levels. SR14 outputs a number of synthetic records of all variables driving TWLs that produce alternate, but physically plausible, combinations of waves and water levels along an identified stretch of coastline~~(see SR14 and Serafin et al. (2017) for more information)~~. This technique is flexible to allow for both the simulation of the present-day climate for computing robust statistics on extreme TWL events, as well as the simulation of future climates and their impact on extreme TWLs.

Because SR14 was developed for use in open-coast environments, it does not include a procedure for simulating estimates of river discharge, ~~important to high water levels in estuarine environments, as well as~~ which is present in the local tide gauge at the La Push study site. SR14 is therefore modified to produce synthetic time series of river discharge as well as a river-induced water level. ~~Specifics of these modifications are presented in section 4.3.~~

4.2 ~~Hybrid modeling of along-river water levels~~

~~The modified simulation technique of SR14 is used to produce 70 500 year long synthetic records representing present-day climate for the time periosd of 1980-2016 of daily maximum SWL and discharge for both the Sol Duc and Bogachiel rivers. Modeling all of the simulated conditions in HEC-RAS in order to output along-river water levels would be prohibitively expensive. As an alternative to time consuming simulations, surrogate models (Razavi et al., 2012) are developed to approximate the response of a HEC-RAS simulation. A large number of combinations of SWL and river discharge at the Bogachiel and Sol Duc rivers are run in HEC-RAS, outputting along-river water level at each HEC-RAS transect. The number of combinations of SWL and river discharge used in the surrogate models are chosen to minimize interpolation errors during validation runs. A surrogate model representing along-river water level is created for each modeled SWL condition using a scattered linear interpolation of the 3D surface of boundary conditions.~~

~~Along-river water levels are extracted from the surrogate model relating to each synthetic combination of SWL and river discharge, providing a longitudinal water surface profile for each day of the 500 year long record in an efficient manner. The large sample size of joint SWL-discharge events ensures a robust, probabilistic estimate of low probability water levels along the Quillayute River. This allows for an exploration of the drivers of along-river water levels over the past 35 years.~~

~~a) The joint relationship between storm surge and wave height for La Push, Washington (black) and Westport, Washington (pink). Example storm surge and discharge relationship at b) La Push and c) Westport, Washington.~~

4.2 ~~Extracting spatially variable return level events~~

~~The new methodology described in this paper allows for a statistically robust estimate of low probability, along-river water levels not observed in the historical record. Typically, return levels are estimated by modeling the estimated 100-yr hydrologic or meteorologic event, and the resulting water level is assumed to be statistically representative of this condition. However, processes driven by multiple variables means that different "sizes" of hydrologic conditions could potentially drive low probability water levels. The 500 year long synthetic records simulated using the modified SR14 allows for the empirical extraction of return level events rather than an estimation from historic records. Using the count-back method, SWL, river~~

discharge, and water level return level events are selected from each record, where the largest, 5th largest, and 10th largest events in each record correspond to the 500-yrHigh discharge events on the two gauged rivers in the watershed, the Sol Duc and Calawah rivers, 100-yr, and 50-yr return levels, respectively, at each transect. This allows for an analysis of spatially-variable, along-river extreme water levels, as well as the ability to map to the jointly-occurring forcings driving the return level water surface. The large sample space of simulated variables permits a comparison of event-based return levels, where the 100-yr water level is determined by the 100-yr forcing, to response-based return levels, where the 100-yr water level is derived.

5 River-influence in the tide gauge

Once the observational SWL at the La Push tide gauge is decomposed, peak η_{SS} events are found to be the highest on record compared to all US West coast tide gauge stations (Serafin et al., 2017). η_{SS} is often found to be jointly related to significant wave height (Hs), where the most extreme η_{SS} occur during storms with associated low pressures, high winds, and high waves. When compared to the relationship of Hs and η_{SS} towards the south in Westport, Washington, many large η_{SS} at La Push occur during small waves, outside of the joint Hs-η_{SS} relationship (Figure 2).

Upon further investigation of the La Push η_{SS} record, almost all instances of extreme η_{SS} events irregular to the joint Hs-η_{SS} relationship are positively correlated with high discharge events. This is inconsistent with η_{SS} in Westport, Washington (Figure 2) and with other tide gauges along the US West coast (not shown). Most tide gauges in Washington and Oregon are situated in bays and estuaries where the estuary volume is much larger than the river input volume. On the other hand, the La Push tide gauge is located on a river discharging directly into the ocean. It is therefore hypothesized that the anomalously large signal in the η_{SS} is indeed river-induced.

Resulting storm surge at the La Push tide gauge modeled using ADCIRC for a simulation including full forcing (red) and a simulation including only discharge and tides (blue) compared to the observed storm surge (black). The ADCIRC simulation was run for the maximum discharge event on record occurring on January 8, 2009.

4.1 Physics-based evidence of river-induced signal

To further investigate the anomalously large η_{SS} at the La Push tide gauge, the hydrodynamic model ADvanced CIRCculation (ADCIRC, Luettich Jr et al. (1992)) and Simulating Waves nearshore (SWAN, Zijlema (2010) model (ADCSWAN; Dietrich et al. (2011)) is used to simulate an example storm event. ADCSWAN has been extensively validated worldwide and has recently found to be skillful for modeling η_{SS} in the PNW (Cheng et al., 2014). ADCIRC is run in 2D depth-integrated barotropic mode which performs well for calculating water surface elevations during storm events (Weaver and Luettich, 2010). SWAN is run in non-stationary mode on an unstructured grid, allowing for tight coupling to ADCIRC.

To test the influence of streamflow on water levels at the tide gauge, the peak streamflow event on record, occurring on January 8, 2009, is simulated. The model is run with two forcing implementations: one including full forcing (e.g., waves, wind, pressure, streamflow, sea level anomalies, seasonality, and tides) and one including only streamflow and tides. Model results show that the simulation including only streamflow and tides is nearly able to recreate the measured η_{SS} signal at the

tide gauge (Figure 7). The addition of wind, pressure, waves, sea level anomalies, and seasonality is found to have minimal impact on the peak observed η_{SS}. Furthermore, maximum peak η_{SS} is found to occur during low tide, indicating a relationship between tide and discharge. While this simulation only explores one instance of this phenomenon, it provides physics-based evidence that anomalously high η_{SS} at this tide gauge is likely being driven by large discharge events.

A comparison of storm surge (η_{SS}) decomposed from all tide gauges along the northern Washington to central Oregon coastline. The solid, black line depicts the regional average of all of the η_{SS} signals, while the dashed black line represents the regional average η_{SS} + 2.5*σ of all η_{SS} in the region. When the La Push η_{SS} exceeds the regional average η_{SS} + 2.5*σ it is removed from the record and considered river influence.

4.1 Removal of river-influence from the oceanographic signal

Storms tend to influence large stretches of coastline at once, and while site-specific variations in the coastline or distance from storm can drive local variations in the amplitude of η_{SS}, the overall η_{SS} signal is fairly coherent across regional tide gauges across the PNW. The river-influenced water levels are therefore isolated and removed from the La Push η_{SS} record by developing a relationship between the La Push η_{SS} and a regionally-averaged η_{SS}.

η_{SS} decomposed from the Neah Bay, Westport, Astoria, South Beach, and Garibaldi tide gauges are averaged each hour to create a regional η_{SS} record (black line; Figure **??**; tide gauge locations in Figure 1). The standard deviation (σ) of the available η_{SS} records at each hour is used to represent the variability of η_{SS} due to local effects at each station. η_{SS} at La Push that are larger than the regional average + 2.5σ are considered anomalous to the region, and defined as river-influenced water levels (η_{Ri}). Observations flagged as larger than the regional average + 2.5σ (dashed line; Figure **??**) were replaced with the regional average + σ. A value of + σ was chosen to minimize jumps in time series when subsituting in a smoother dataset. While this methodology does not remove all the effects of η_{Ri} in the η_{SS} signal, it captures the majority of anomalous water levels driven by high discharge events.

η_{Ri} is produced from the difference between the original La Push η_{SS} and the η_{SS} modified described above which removes η_{SS} anomalous events. η_{Ri} occurring during low discharge events (here low is defined as less than 10 m^3s^{-1}, the approximate summer average discharge) is added back into the La Push η_{SS}, as it is likely not driven by river forcing. After η_{Ri} was removed from the η_{SS} signal, it is saved as a time series of river-forced water level events.

4.1 SR14 modifications for estuarine environments

SR14 was originally developed to simulate TWLs in a Monte Carlo sense in open-coast environments and does not have a mechanism in place for simulating the new variables of interest, river discharge (Q) and η_{Ri}. SR14 was therefore modified to include simulations of η_{Ri} and Q at both the Calawah and Sol Duc rivers. To do this, relationships were formed with variables already simulated within the SR14 model.

High discharge events in the Sol Duc and Calawah (and therefore Bogachiel) riverstend to occur within hours of peak wave events recorded in offshore wave buoy records and water level events recorded in the tide gauge data. Due to the interrelated nature of these forcings, daily maximum estimates of Q at the Calawah River Calawah River discharge (Q_C) are compared

to all variables simulated in the SR14 model (e.g., ~~Hs~~wave height, η_{SS}, η_{NTR}, η_{MMSLA}~~, etc.~~) to capture any ~~dependency inherent in~~ dependencies between these processes. The ~~most correlated variable to Q is Hs.~~

~~Similar to methods in SR14, extreme Hs and Qevents at the Calawah River are determined using the Peak Over Threshold approach, where all independent daily maximum events over a defined threshold are selected. Threshold excesses are fit to non-stationary Generalized Pareto distributions, which include seasonality as a covariate. Both variables are transformed to approximately Fréchet margins. A bivariate logistics model is then used to model the dependency between the variables. To simulate, random numbers are sampled from a uniform distribution and mapped to each variable's prescribed Fréchet cumulative probability distribution function. Based on the probability~~ variable with the highest monthly correlation to Q_C is wave height (Hs). Extreme Q_C events are simulated using a bivariate logistic model, which is the same technique used to simulate η_{SS}. The bivariate logistic model preserves the dependency and frequency of occurrence of ~~the transformed value, the estimate is transformed back to the physical scale using the Generalized Pareto distribution if extreme , dependent on the variable's threshold. If not extreme, the estimate is transformed back to the physical scale using monthly-varying Gaussian copulas.~~ joint Hs-Q events in extreme and non-extreme space. This technique generates a synthetic record of Q~~at the Calawah River gauge~~ $_C$ that is seasonally varying, related to larger-scale climate variability through wave height (essentially as a proxy for storms), and carries the same dependency between variables as the observational record (Figure 4a). Q_C is then multiplied by 2.09 to represent inflow from both the Bogachiel and Calawah rivers. ~~The bivariate logistic model preserves the dependency and frequency of occurrence of joint Hs-Q events in extreme and non-extreme space. This modeling technique is also used to simulate η_{SS} in SR14.~~

~~Because discharge~~ Discharge measurements at the Sol Duc River are highly correlated with the discharge measurements at the Calawah River (ρ = 0.9, τ = 0.83), ~~the~~ thus Sol Duc River discharge (Q_{SD}) is modeled based on a relationship with the ~~Calawah River. Once the Calawah River is scaled to represent~~ scaled Q_C, representing the Bogachiel River ~~, estimates of Qat the Sol Duc River~~ (Q_B). Estimates of Q_{SD} are related to ~~the Bogachiel River~~ Q_B during the summer and winter seasons. First, daily maximum Q is split into summer (May, June, July, August, September, and October) and winter (January, February, March, April, November, December) seasons. Next, ~~two~~ models are fit to the joint relationship between the ~~Sol Duc River Q(hereinafter Q~~Q_{SD} ~~) and the Bogachiel River Q(hereinafter Q~~and Q_B ~~)~~ each season, such that for the summer season, ~~a best-fit linear model represents Q_{SD}~~

$$Q_{SD} = 1.186 Q_B + 0.226. \quad (1)$$

is used when Q_B falls between 0-10 $m^3 s^{-1}$, and ~~a best-fit quadratic represents Q_{SD}~~

$$Q_{SD} = -1.0 \times 10^{-4} Q_B^2 + 0.38 Q_B + 14.07. \quad (2)$$

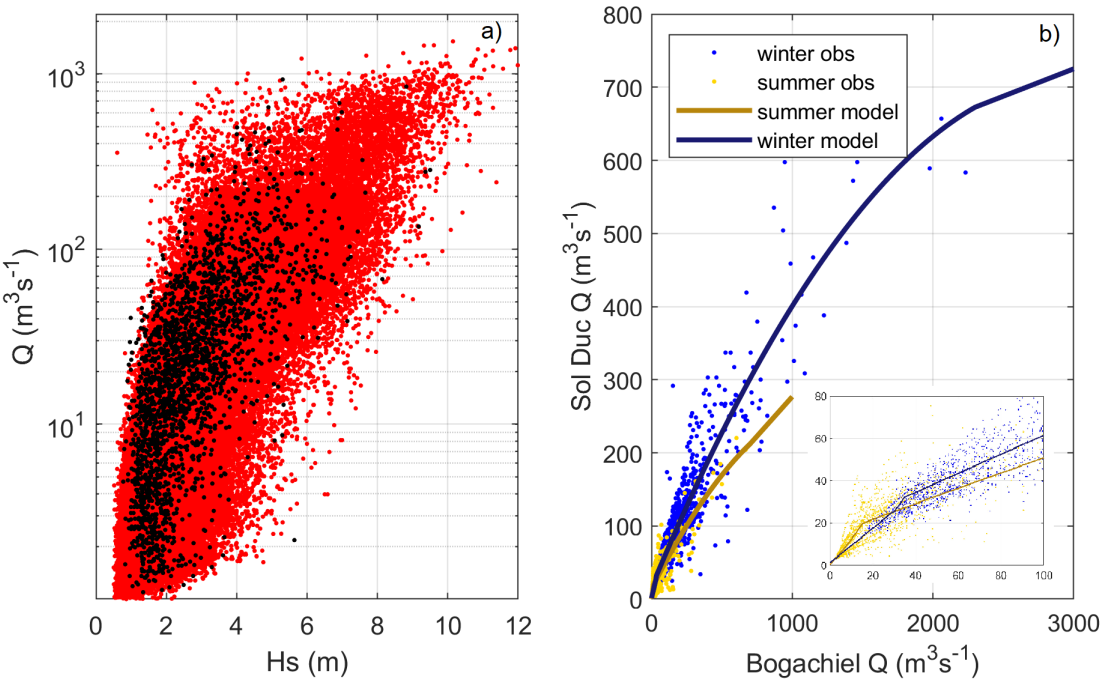

Figure 4. a) Joint relationship between wave height (Hs) and ~~storm surge and~~ discharge (Q) for the observational record (black) and one example 500 year simulation (red). b) Seasonal model fit for the probabilistic simulation of the Sol Duc River Q in relation to the Bogachiel River Q. The inset displays the model fits for discharge less than ~~30~~ 100 m^3s^{-1}.

is used when Q_B falls between 10 - 700 m^3s^{-1} (Figure 4~~). b~~). When Q_B is greater than 700 m^3s^{-1}, Q_{SD} is determined using

$$Q_{SD} = 0.216Q_B + 61.25. \quad (3)$$

For the winter ~~model, a linear model is fit to Q_{SD}~~ season,

$$Q_{SD} = 0.816Q_B + 1.168. \quad (4)$$

is used when Q_B ~~fell between 0-30~~ falls between 0-25 m^3s^{-1}, and ~~a quadratic~~

$$Q_{SD} = -1.0 \times 10^{-4}Q_B^2 + 0.46Q_B + 16.11. \quad (5)$$

when Q_B falls between ~~30~~ 25 - 2300 m^3s^{-1} (Figure 4~~). Equally spaced bins are determined and~~ b). When Q_B is greater than 2300 m^3s^{-1}, Q_{SD} is determined using

$$Q_{SD} = 0.075Q_B + 500.42. \quad (6)$$

Summer and winter Q_B is binned and residuals of Q_{SD} from the above model fits are generated. Normal distributions are fit to ~~the~~ Q_{SD} residuals in each bin, except for low bins (less than ~~30~~ 25 m^3s^{-1}) where residuals are fit to exponential distributions. Q_{SD} is then directly related to simulated estimates of Q_B; Q_{SD} is first determined by fitting the prescribed model to each estimate of Q_B, and then a random sample is taken from the residuals per ~~that bin~~ binned Q_B and added to the model. This technique captures the joint-peaks of the river systems visible in the observed dataset, while allowing for variability ~~in~~ between the simulated estimates (Figure 4b).

~~The largest η_{Ri} usually occur coincident with low tide . This is likely due to the competing ocean and river processes during high Q events. During high tide, riverine floodwaters are blocked from outletting to the ocean and back up in the river. As the water recedes during low tide, the river is no longer suppressed and exits through the inlet (Kumbier et al., 2018; Chen and Liu, 2014) . The drainage of the river into the ocean generates high water levels at the mouth, elevating the SWL during low tide, driving a peak in the η_{NTR}. ADCIRC simulations confirm this phenomenon, as the river discharge peak is modeled exactly at low tide (Figure 7). We are, however, most interested in the~~

4.0.1 Modeling the river-induced water level

At tide gauges along the US West coast, the maximum daily SWL ~~that drives flooding, which~~ generally occurs during, or close to, the daily high tide ~~. Modeling large~~ (Serafin and Ruggiero, 2014; Serafin et al., 2017). Modeling peaks in η_{Ri} that occur during low tide would therefore erroneously increase simulated estimates of the SWL occurring during high tide. Thus, instances of η_{Ri} occurring approximately during high tide are retained and all other η_{Ri} peaks are discarded~~. The resulting~~ , resulting in 155 ~~peaks in η_{Ri} are correlated with Q_B (Figure 5)~~events.

~~In order to statistically simulate~~ Synthetic estimates of η_{Ri} ~~, two linear regression models are fit to~~ are developed by relating Q_B and η_{Ri}~~, where Q_B is the independent variable. Two models rather than one are chosen because the elevation of η_{Ri} increases and becomes more varied as Q_B increases. The first linear model is fit to~~ . This relationship is modeled using

$$\eta_{Ri} = 0.039Q_B + 0.854 \times 10^{-3}. \quad (7)$$

when Q_B is below 190 m^3s^{-1} ~~, and the second is fit to~~ and

$$\eta_{Ri} = 0.093Q_B + 0.284 \times 10^{-3}. \quad (8)$$

when Q_B is above 190 m^3s^{-1} (Figure 5a). Next, coarse bins ranging from 100 to ~~400~~ 4000 m^3s^{-1} are created and the standard deviation (σ) of η_{Ri} ~~values~~ within each bin is saved. For bins that ~~contained~~ contain less than 10 observations, observations

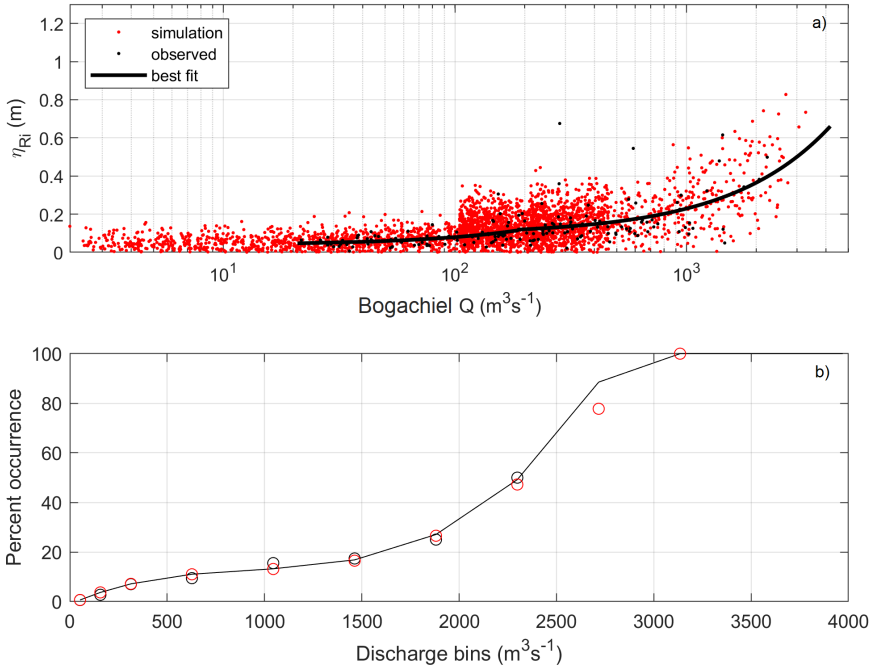

Figure 5. a) The relationship between the river-influenced water level (η_{Ri}) and ~~river~~ Bogachiel River discharge ~~(Q)~~on a log-linear scale. The solid black line represents the ~~linear~~ model fit to the observational records (black dots). b) The percentage of time η_{Ri} occurs in the record during a specific Q_B. In both panels, black represents the observational record and red represents one example 500 year simulation.

from the previous bins ~~were~~ are included until there ~~were~~ are more than 10 observations per bin for σ calculations. Finally, a 2-point running average ~~was~~ is used to smooth ~~the~~ σ from each bin to ensure continuous transitions and to avoid the edge-effects from binning a sparse dataset. ~~After Q_B were simulated using SR14, the developed modification simulates η_{Ri} for every day in time by selecting the synthetic daily estimate of Q_B and randomly sampling from a normal distribution for each Q_B bin, where the distribution parameters are modeled as μ = the regression model and σ = the standard deviation from each bin (Figure 5).~~

There are times of high Q_B without a distinguishable η_{Ri} in the tide gauge record, thus a model is also developed to simulate the frequency of occurrence of η_{Ri} ~~as not to artificially elevate~~ during daily maximum SWLs. The frequency of occurrence of η_{Ri} is ~~therefore~~ defined as the percentage of time η_{Ri} occurs in the observational record~~. In the observational record, η_{Ri} occurs~~ , which is less than 10% of the time when Q_B is less than 210 m^3/s, and 15 - 25% of the time when Q_B is between 840 and 2090 m^3s^{-1} (Figure 5b). For Q_B greater than 2090 m^3s^{-1}, η_{Ri} occurs ~~during daily maximum water levels~~ approximately 50% of the time. ~~Estimates of the percentage of time~~ The frequency of occurrence of η_{Ri} ~~occurs are modeled by~~ is modeled using a best-fit cubic function~~to the~~ , where the frequency of occurrence is a function of Q_B based on the percentage of time the values have occurred in the record. Because there ~~is no record of~~ are no events greater than 2500 m^3s^{-1} on record, we

represent the percentage of occurrence over this value as 100% ~~, because at some point, large Qevents would drive~~ (Figure 5b).

Once Q_B is simulated using SR14, η_{Ri} ~~to occur 100% of the time~~ is simulated for every day in time by selecting the synthetic daily estimate of Q_B and randomly sampling from a normal distribution for each Q_B bin, where μ is the regression model and σ is the standard deviation from each bin (Figure 5a). The ~~example simulationshows SR14 captures~~ frequency of occurrence model is then used to select the correct proportion of η_{Ri} events to retain for each synthetic simulation. These techniques capture both the spread of η_{Ri} related to Q~~events~~ $_B$ as well as the percentage of time of occurrence (Figure 5).

4.1 Hydraulic model for along-river water levels

While a variety of hydraulic models can be used for determining the elevation of along-river water ~~level for the worst performing condition in the validation tests.~~ levels, we employ the Hydraulic Engineering Center's River Analysis System (HEC-RAS; Brunner (2016)). HEC-RAS is used to estimate water surface elevations in rivers and streams in both steady and unsteady flow and under subcritical, supercritical, and mixed flow regimes (Goodell, 2014). HEC-RAS has been previously used to model water surfaces for a range of applications including, but not limited to, floodplain mapping (Yang et al., 2006), flood forecasting (Saleh et al., 2017), dam breaching (Butt et al., 2013), and flood inundation (Horritt and Bates, 2002). HEC-RAS computes water levels by solving the 1D energy equation with an iterative procedure, termed the step method, from one cross-section to the next (Brunner, 2016). For subcritical flows, the step procedure is carried out moving upstream; computations begin at the downstream boundary of the river and the water surface elevation at an upstream cross-section is iteratively estimated until a balanced water surface is obtained. Energy losses between cross-sections are comprised of a frictional loss via the Manning's Equation and a contraction/expansion loss via a coefficient multiplied by the change in velocity head (see Brunner (2016) for more details).

In this application, HEC-RAS is used to model 1D water levels under gradually varied, steady flow conditions at transects along the Quillayute River. While a simplification of flood processes, the 1D application is commonly used to create flood hazard maps. A detailed Digital Elevation Model (DEM) is developed for the river network, including bathymetry and topography for the floodplains of interest (Figure 6). Model domain boundary conditions are chosen as the SWL at the tide gauge (m; downstream boundary) and river discharge from the Sol Duc and Bogachiel rivers (m^3s^{-1}; upstream boundary). The HEC-RAS model is validated using water surface measurements from a 2010 survey. Details of the HEC-RAS model validation and calibration procedures are documented in supplemental information.

4.2 Hybrid statistical-physical modeling

The modified simulation technique of SR14 is used to produce 70 500 year long synthetic records representing present-day climate for the time period of 1980-2016 of daily maximum SWL and Q for both the Sol Duc and Bogachiel rivers. Rather than run the ~13 million conditions simulated through a numerical model, a limited set of joint boundary conditions of SWL and Q (at the Bogachiel and Sol Duc rivers) are run through HEC-RAS, outputting the elevation of the along-river water level at each HEC-RAS transect. Surrogate models are generated from the HEC-RAS runs for each transect using a scattered

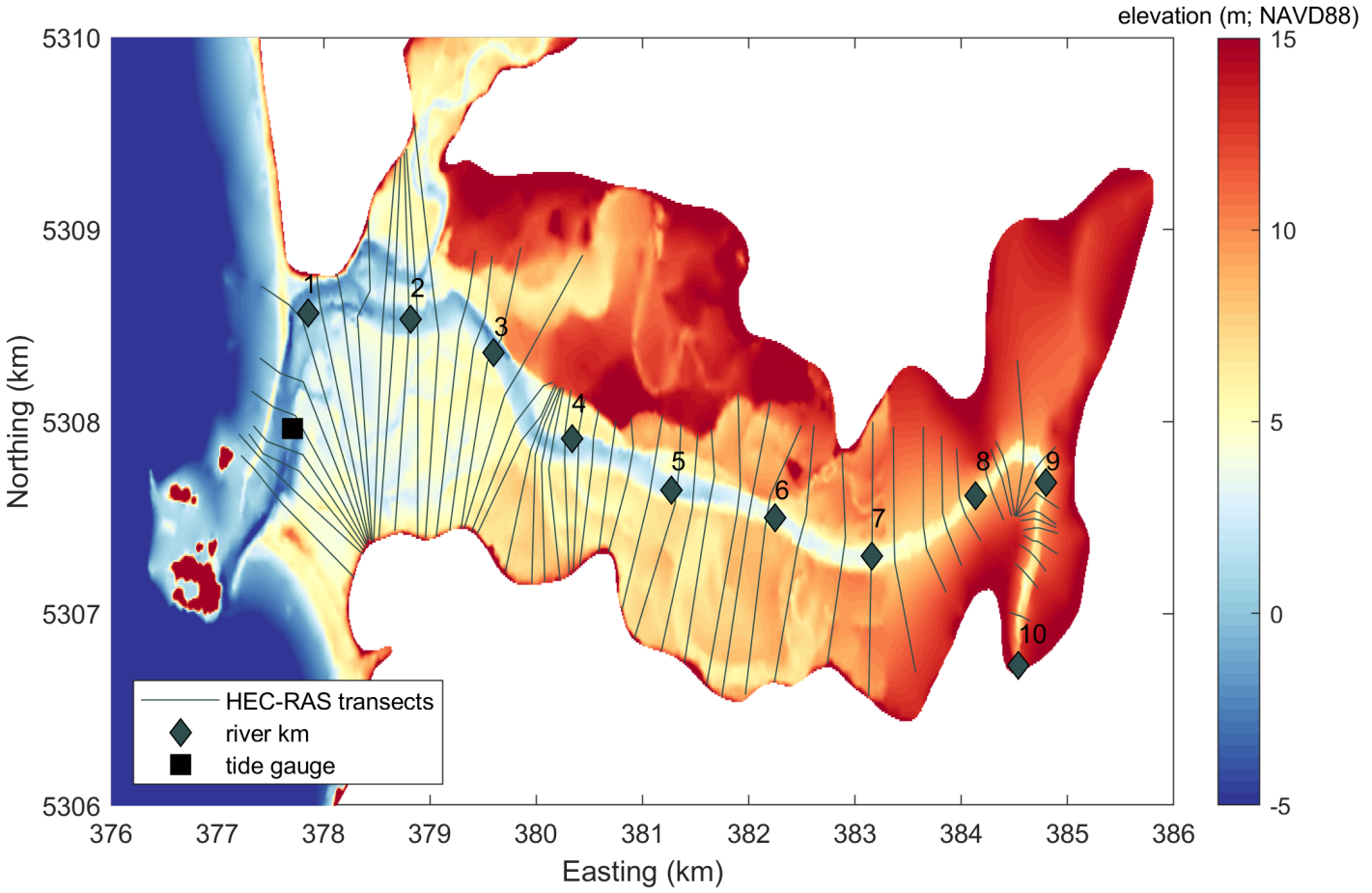

Figure 6. ~~a) Modeled HEC-RAS Q boundary conditions used to generate the surrogate models~~ Digital Elevation Model (~~red-dotted lines~~DEM) ~~compared to the simulated conditions~~ used for ~~surrogate model validation (green dots). The black dots represent~~ the ~~observational daily max conditions, while the colored circles represent the worst-performing~~ HEC-RAS simulations of the ~~validation tests~~Quillayute River. ~~The red~~ HEC-RAS cross sections are depicted as grey lines. Approximate river kilometer and ~~blue colored circles represent~~ the ~~scenarios where the interpolated water surface had a bias~~ location of ~~over 10 cm lower than~~ the ~~model~~tide gauge are depicted as diamonds and a square, respectively.~~b) Example~~

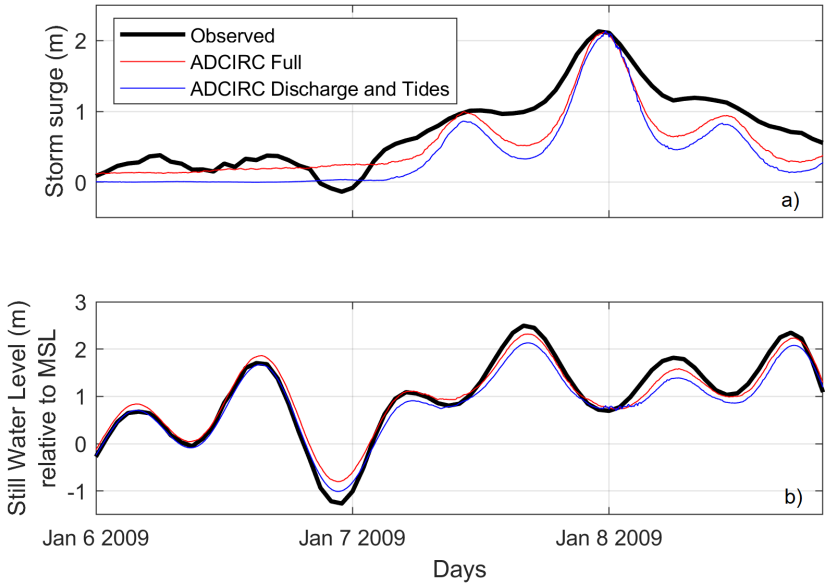

Figure 7. Resulting storm surge (a) and still water level (b) at the La Push tide gauge modeled using ADCIRC for a simulation including full forcing (red) and a simulation including only discharge and tides (blue) compared to the observed storm surge (black). The ADCIRC simulation was run for the maximum discharge event on record occurring on January 8, 2009.

linear interpolation of the 3D surface of boundary conditions. The number of combinations of SWL and Q used to develop the surrogate models are chosen to minimize interpolation errors during validation runs. A daily estimate of water level elevation at each transect is produced by inputting all daily maximum SWL and Q conditions into the surrogate models, which efficiently extract along-river water levels for any set of SWL and Q inputs. Using the countback method, where for example, the 5th largest event for each synthetic record would by the 100-yr event, water level return levels are extracted for all 70 500 year synthetic records for the 1) along-river water levels at each transect, 2) SWLs, and 3) Q. This methodology provides both an estimate of the return level magnitude (e.g., the average of the 70 100-yr events), as well as the uncertainty around that magnitude (e.g., the distribution of the 70, 100-yr events). It also provides a technique to compare the response-based return level (e.g., the 100-yr water level) to the event-based return level (e.g., water level driven by the 100-yr SWL or 100-yr Q event).

5 Results

~~The following section first provides a validation of the surrogate models by comparing~~ The following section first validates the presence of a river-induced water level within the tide gauge signal, then demonstrates the effectiveness of the surrogate models in representing along-river ~~water levels from a specific set of conditions directly modeled in~~ water levels for unmodeled

HEC-RAS ~~to along-river water levels interpolated from the surrogate models for the same set of~~ boundary conditions. Next, the spatial and temporal variability of the magnitude of along-river water levels and their driving conditions are examined. Finally, low probability water levels, like the 100-yr event, are extracted ~~and their~~ from the simulated records of along-river water levels and the dominant drivers are evaluated~~and compared to the low probability water level from the 100-yr dischargeor 100-yr SWL event at each transect~~.

5.1 River-induced water level validation

Results from ADCSWAN modeling of the January 8, 2009 storm event show that the simulation including only river discharge and tides is nearly able to recreate the measured peak η_{SS} signal at the tide gauge (Figure 7a). The addition of wind, pressure, waves, sea level anomalies, and seasonality is found to have minimal impact on the peak observed η_{SS}. Furthermore, the maximum η_{SS} occurs during low tide (Figure 7b), which indicates a potential relationship between water surface elevation, tidal level, and river discharge. While the ADCSWAN runs only explore one instance of this phenomenon, it provides physics-based evidence that anomalously high η_{SS} at the La Push tide gauge is likely being driven by large discharge events.

5.2 Surrogate ~~models~~model validation

~~Approximately 3,000 Q-SWL~~ A number of validation scenarios are ~~directly modeled through~~ modeled in HEC-RAS to determine ~~if the number of conditions used for surrogate model generation~~ whether the combinations of Q and SWL boundary conditions used to develop the surrogate models represent a large enough sample space of forcing conditions for ~~correctly interpolating~~ the interpolation of along-river water levels. The validation scenarios are chosen to cross through both HEC-RAS modeled and unmodeled conditions (Figure 8a). Across all validation scenarios, the average root mean square error (RMSE) between the HEC-RAS directly-modeled and ~~surrogate model-generated water level~~ the surrogate model-interpolated water levels is 1 cm. Only ~~about~~ 1.5% of the validation scenarios have a bias greater than 10 cm, and the largest RMSE at any transect is 20 cm across all ~~water level~~ scenarios (Figure 9). The ~~worst represented scenarios occur during high Bogachiel River Qevents~~ validation scenario with the worst performance occurs during high Q_B and low Q_{SD} paired with low ~~Sol Duc River Q and low~~ SWL events. However, even during ~~these cases~~this case, the differences between the HEC-RAS directly-modeled the surrogate model-interpolated ~~and directly modeled water levels are~~ water level is small (Figure 8b). The main research ~~interest~~ focus here is extreme water levels, and the conditions driving low probability return level events rarely ~~fell~~ fall around the scenarios with the highest bias.

~~a) Variability of along-river water levels averaged over summer (JJA), fall (SON), winter (DJF) and spring (MAM). b) The difference between the fall, winter, and summer and the spring along-river water level.~~

~~Left) Observational (black) and simulated (red) monthly median still water level (SWL), non-tidal residual (η_{NTR}), and discharge (Q). Right) Observational (black) and simulated (red) monthly 98th percentile of the SWL, Q, and η_{NTR}. Red shading indicates the bounds value from each simulation.~~

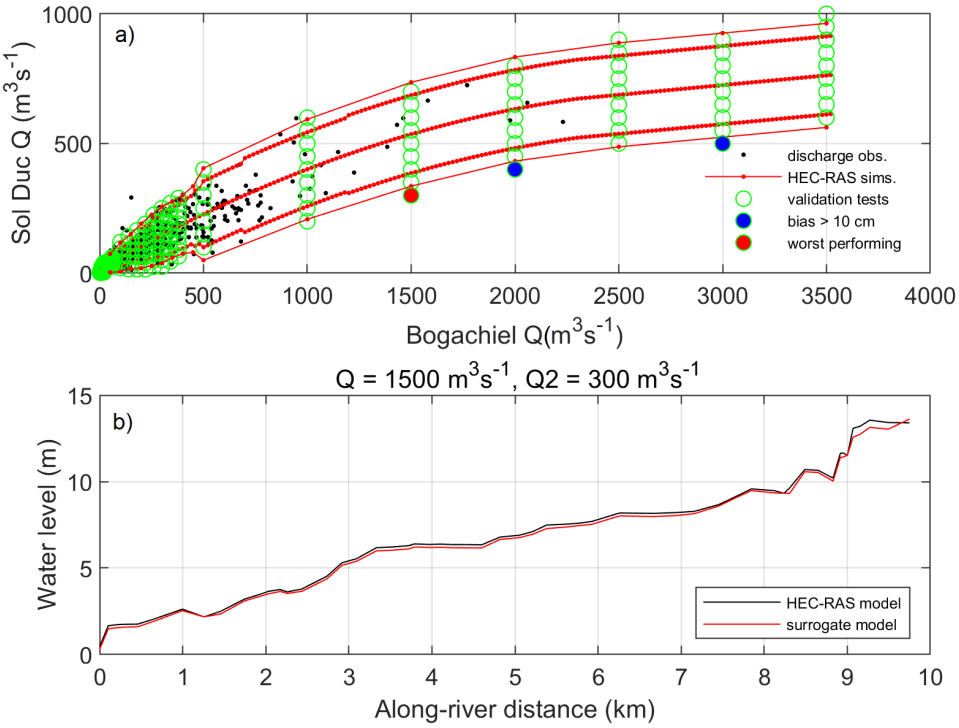

Figure 8. a) Modeled HEC-RAS Q boundary conditions used to generate the surrogate models (red-dotted lines) compared to the simulated conditions used for surrogate model validation (green dots). The black dots represent the observational daily max conditions, while the colored circles represent the worst-performing of the validation tests. The red and blue colored circles represent the scenarios where the interpolated water surface had a bias of over 10 cm lower than the model. b) Example along-river water level for the worst performing condition in the validation tests.

5.3 ~~Temporal variability in~~ Hybrid modeling of along-river water levels

~~Similar to the driving boundary conditions of SWL and Q, seasonal~~

5.3.1 Temporal variability

Seasonal variability exists in the elevation of along-river water levels. The highest elevation water level occurs during the winter (here defined as December, January, ~~and~~ February), while the lowest elevation water level occurs during the spring (March, April, May) (Figure 10a). The spring ~~profile~~ along-river water level is on average ~~(maximum difference) 50 cm (84 cm)~~ 0.50 m lower than the winter ~~profile, 33 cm (63 cm)~~ along-river water level, 0.33 m lower than the fall (September, October, ~~and November) profile, and 3 cm (12 cm)~~ November) along-river water level, and 0.03 m lower than the summer (June, July, ~~and~~

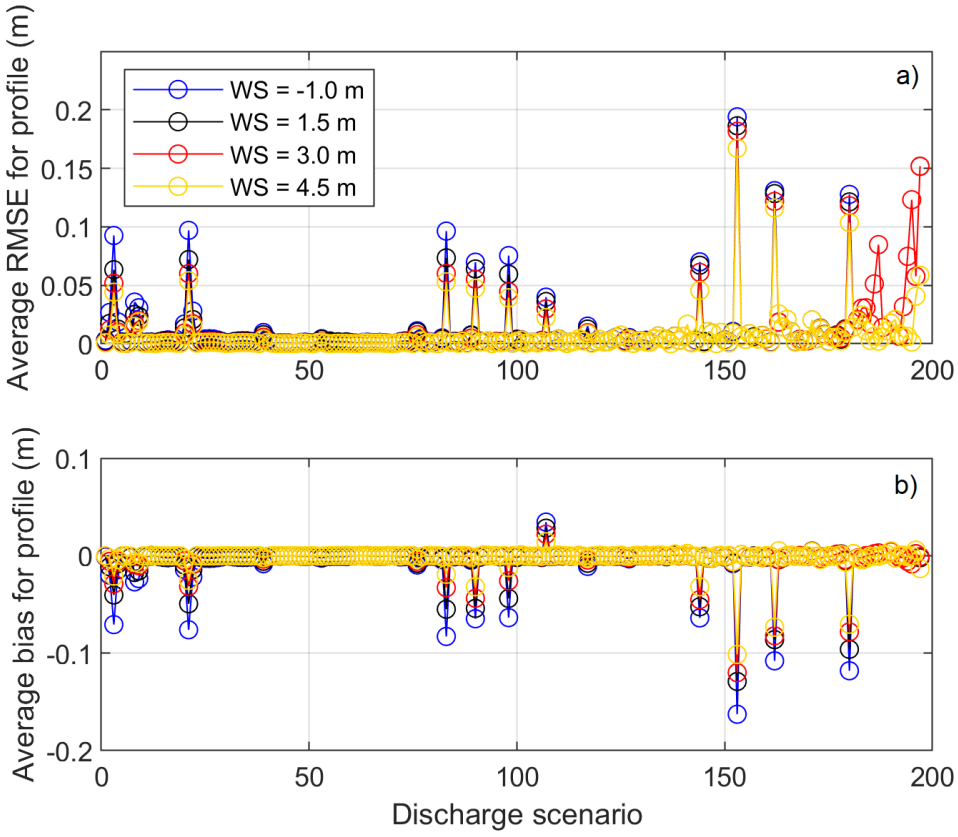

Figure 9. a) Average root mean square error (RMSE) and b) bias for all 197 discharge validation scenarios ~~(e.g., 197 Q and~~ across 4 out of the 15 SWL ~~) across four SWL~~ scenarios. The worst-performing model ~~(pictured in the previous figure)~~ is discharge scenario 153.

~~August) profile~~ August) along-river water level (Figure 10b). The difference between seasonal ~~profiles~~ along-river water levels is nonlinear upstream, and certain sections of the river have larger changes in elevation between months (Figure 10b). However, this variation becomes relatively linear downstream of river km 3.

The seasonal variability of the along-river water level is driven by the seasonality of the forcings, which are well represented in the simulations compared to the observations (Figure 11). The ~~median Q of the Quillayute (combined Sol Duc and Bogachiel Q) is approximately 200 m^3s^{-1} higher in winter months than summer months (Figure 10~~monthly median SWLs and η_{NTR}s are higher in the winter than in the summer (Figure 11a and Figure 11b). This cyclical variability is also depicted in the monthly median ~~SWL and η_{NTR}. Winter η_{NTR} is approximately 40 cm higher than summer η_{NTR}, which is also reflected in the SWLs (a and b, Figure 11~~river discharge from the Quillayute River (combined Sol Duc and Bogachiel Q), and is approximately 200 m^3s^{-1} higher in winter months than summer months (Figure 11c). The 98th percentile of ~~Q, SWL, and~~ SWL, η_{NTR}, and Q have a similar seasonal variability as the median conditions (Figure 11d, Figure 11e, and Figure 11f).

5.4 ~~Probabilistic spatially-varying extreme water levels~~

~~Using the count-back method,~~

5.3.1 Spatial variability

The large number of joint SWL and Q conditions allows for the direct extraction of water level return ~~level events at each transect are extracted for all 70 500 year long simulations representing present-day climate from 1980-2016. This methodology thus provides both an estimate of the average water level return level as well as the uncertainty around that value.~~ levels and the corresponding univariate or multivariate drivers along each HEC-RAS transect. The magnitude of ~~along-river water level return level events are between 2 and 10 m, with peaks near 1~~the 100, 25, 10, and annual return level water levels is between 3 and ~~9 km (Figure 12~~17 m (NAVD88, Figure 12a). While the peaks in ~~water level~~ return level events occur at similar locations, the difference between ~~water level~~ return level events ~~spatially varies~~ varies spatially moving upriver. For example, at river km 1, the difference between the average (of all simulations) annual and 100-yr event is approximately ~~50 cm~~0.9 m, whereas at river km ~~9.5~~8 and upstream, the difference between ~~the~~ these two events is closer to 2 m (Figure 12b).

~~The many realizations of joint SWL-Q allows for the investigation of the fluvial and oceanographic processes driving the magnitude of~~

The dominant forcing conditions driving water level return ~~level events. Panels c and d in Figure 12 displays the average condition forcing the water level return level for the annual, 25, 100, and 500-yr event . Between river km 0 and 1.5, the average SWL driving the water level return level eventis constant and then gradually decreases over a 1 km zone by approximately 50 cm. On the other hand, the~~ levels varies along-river. At the river mouth, the annual water level event (e.g., the event that is expected every year) in each simulation occurs during Q ranging from 40 - 2600 m^3s^{-1} and SWLs around 3.3 m, which corresponds with the annual SWL event (Figure 13a). Moving upstream to river km 1 and 2, the annual water level event is driven by both high SWL occurring during low Q and low SWL occurring during high Q. At river km 4, the annual water level event occurs during the annual Q event coincident with SWLs that range from 1.8 - 3.9 m (Figure 13a). These results are similar, albeit events are larger magnitude, for the 100-yr water level event. Downstream 100-yr water levels are driven by SWLs, upstream 100-yr water levels are driven by Q, and the 100-yr water level between km 1 and 2 is driven by different combinations of high and low SWL and Q events (Figure 13b).

The relative importance of both oceanic and riverine forcing to extreme water levels emerges when averaging the magnitude of the drivers of the water level return levels at each transect from all 70 500 year long simulations (Figure 14). The magnitude of the average Q driving ~~the~~ water level return ~~level event~~ levels gradually increases by approximately ~~2000~~ 1000 m^3s^{-1} over river km 0 - ~~3~~ 2 and then is ~~fairly constant~~ consistent from river km ~~3~~ 2 to 10 (Figure ~~12). Compared to the univariate return level forcings,~~ 14a). Downstream, between river km 0 and 0.25, the magnitude of the average SWL driving water level return levels is consistent and then gradually decreases over a 1 km zone (Figure 14b).

When comparing to water level return levels driven by a univariate forcing or event return level (e.g., along-river water levels modeled from the 100-yr Q or SWL event), we find that the stretches of river ~~that display constant~~ driven by a consistent SWL

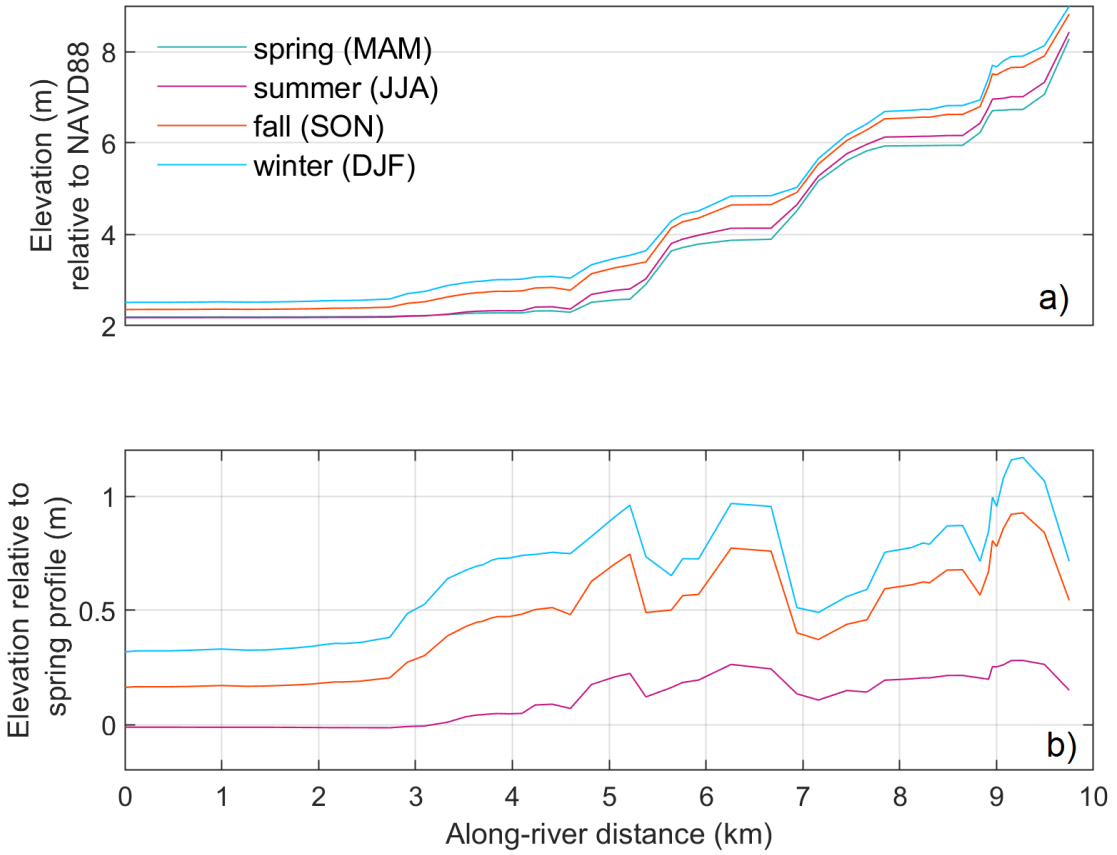

Figure 10. a) Variability of along-river water levels averaged over spring (MAM), summer (JJA), fall (SON), and winter (DJF). b) The difference between the spring and summer, fall, and winter along-river water levels.

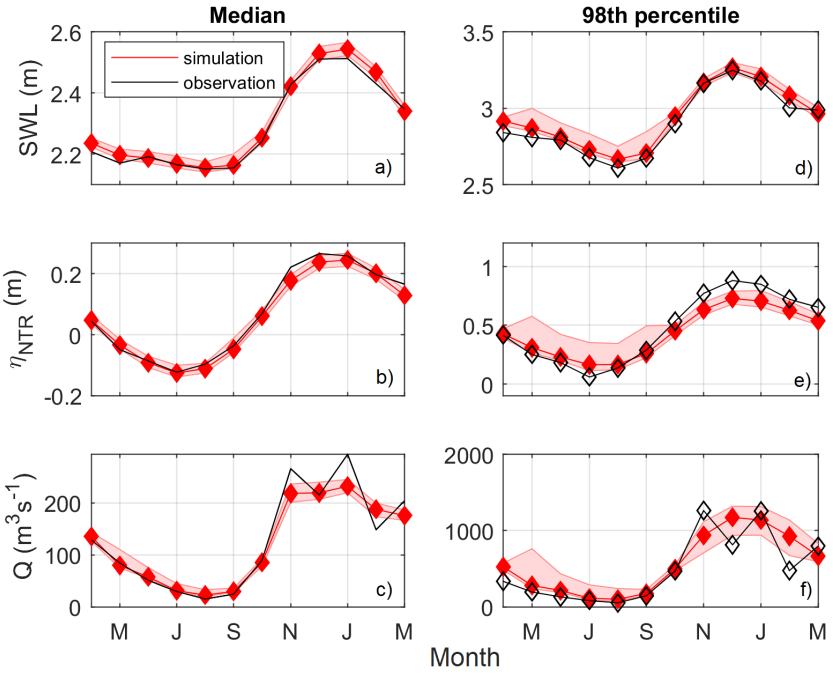

Figure 11. Left) Observational (black) and simulated (red) monthly median still water level (SWL), discharge (Q), and non-tidal residual (η_{NTR}). Right) Observational (black) and simulated (red) monthly 98th percentile of the SWL, and η_{NTR} Q. Red shading indicates the bounds value from each simulation.

or Q forcing ~~approximate~~ approximates the univariate return level event~~such that~~ . Therefore, the 100-yr SWL does indeed cause the 100-yr water level ~~in the lower river near the ocean outlet~~downstream, between river km 0 and 0.25, while the 100-yr Q event drives the 100-yr water level ~~along river km 3~~ upstream, between river km 2 - 10 (~~grey~~ dashed lines, Figure ~~12~~14). However, between river km ~~1.5~~ 0.25 - ~~2.5~~ 1.75 a flood transition zone is present, where neither the SWL return level or the Q return level ~~drives~~ events drive the water level return level. This is consistent across all return level events~~, regardless of likelihood. This is further evidenced by investigating the SWL and Q conditions that drive the annual and 100-yr event at specific along river transects (Figure 13). At the river mouth, the annual water level event occurs during Q ranging from 20 - 3200 m^3s^{-1} and SWLs that vary by only 10 cm. Moving upstream to river km 2, which lies in the flood transition zone, the annual event is driven by both high SWL occurring during low Q and low SWL occurring during high Q. By river km 4, the annual event is forced by the univariate, annual Q event (Figure 13). This pattern is similar for the 100-yr event at all transects but with higher magnitude SWL and Q conditions.~~ .

~~a) The average along-river water level return level at each transect for all 70 probabilistic simulations. b) The along-river difference between the average annual and 100-yr event. The average forcing condition driving the response-based return level at each river transect where c) displays the Quillayute Q scenario driving low probability water levels and d) displays the~~

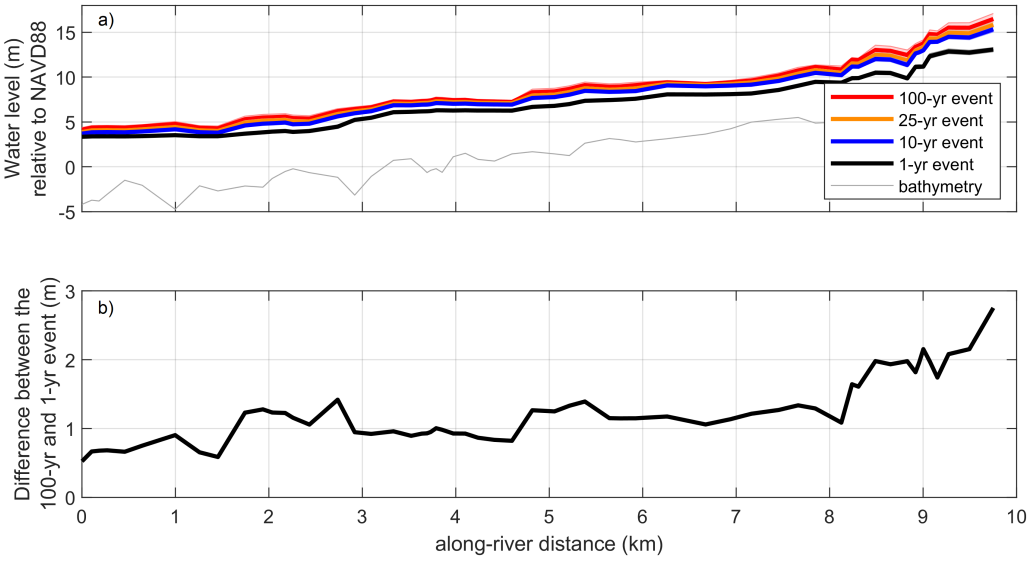

Figure 12. a) The water level return level at each transect for all 70 probabilistic simulations. Each return level event displays the average of the simulations (solid line) as well as the range around the average (shaded). b) The along-river difference between the annual and 100-yr event, averaged over 70 simulations.

~~SWL scenario driving low probability water levels. The grey dashed lines depict the event-based return level, where the low probability water level would be modeled based off , for example, the low-probability discharge. Red, orange, blue, and black lines represent the 500, 100, 25, and annual return level event. In panels c and d, the pink shaded area represents a transition zone, where neither event drives the water level.~~

6 Discussion

The hybrid model developed in this study, which combines statistical simulations with a physics-based model, provides ~~a novel~~ an approach for probabilistically evaluating the conditions that drive extreme water levels, not only ~~at a tide gauge~~in an open-coast setting, but also miles upriver. The ability to simulate ~~hundreds of thousands of~~ millions of combinations of Q and SWL events allows for a robust estimate of resulting along-river water levels, which numerical models alone are unable to consider due to large computational expenses. While some of our modeling techniques are specific to this location, the overall framework for combining statistical and physics-based models is general enough for use in coastal locations throughout the globe where flooding arises from compounding processes.

The decomposition of the SWL into low and high frequency signals, including a river-influenced component, helps ~~characterize~~ identify the importance of physical processes ~~in~~ for generating high water levels across various regional settings. This is especially important in locations like the US West coast, where the steep, narrow continental shelf prevents wind and pressure

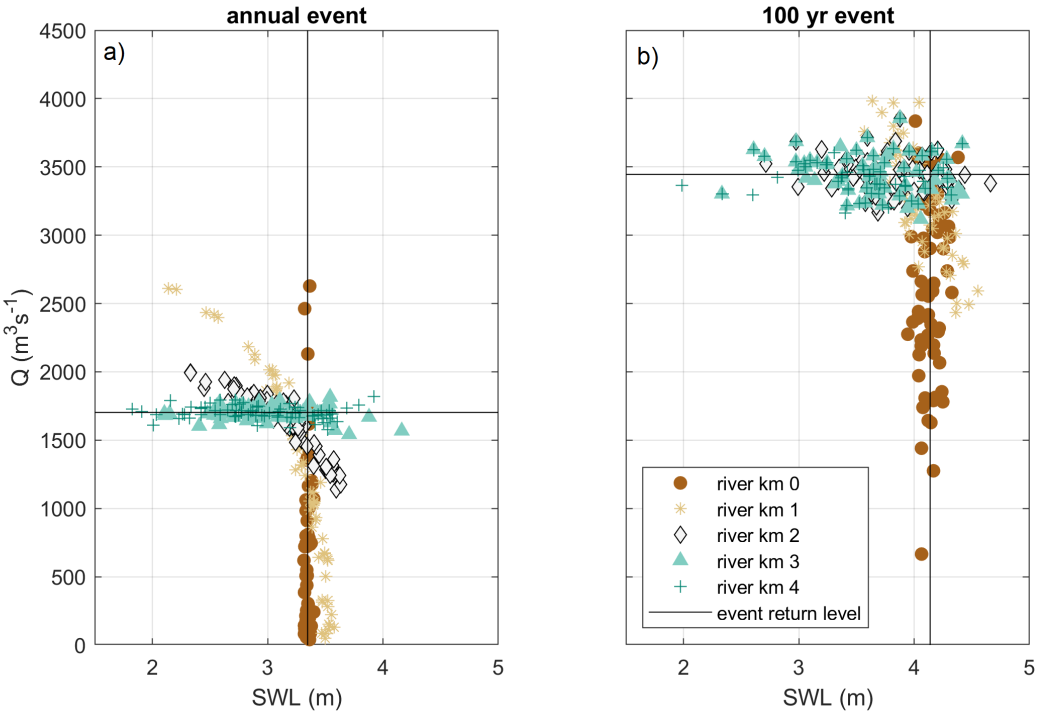

Figure 13. The individual Q or SWL condition driving the a) annual and b) 100-yr water level event at specific along-river locations for each 70 500 year simulation. In both figures, the black lines represent the annual and 100-yr return level magnitude for Q and SWL.

driven storm surge from being overwhelmingly large (Allan et al., 2011). The influence of the river signal in the tide gauge is directly related to the setting of our study site. The estuary is relatively small and narrow with the river discharging directly into the ocean. This is dissimilar to other tide gauges in the region which are located in larger estuaries, situated away from river input. Estuaries typically exhibit wave, tide, or river-dominant morphology, based on the relative energy of each process (Dalrymple et al., 1992). The Quillayute River outlets directly to a high wave energy environment and has a small estuary volume compared to its river input volume. The steep catchment of the mountainous environment means a short response time for rainfall, therefore producing peak discharges temporally similar to peak storm-induced still water levels, allowing for interaction between the two. In contrast, water level elevations with large estuary volume compared to river discharge are less influenced by fluvial processes. Furthermore, a larger estuary may experience variability in the water surface elevation due to wave-induced setup and/or other local storm-induced processes (Cheng et al., 2014; Olabarrieta et al., 2011), which may further dampen the influence of a river signal.

~~Defining compounding extreme events based on a more complete probability space of jointly-occurring conditions has been described in open coast settings (Serafin et al., 2017), however this is the first application to riverine environments.~~ This research confirms the presence of an oceanographic-fluvial transition zone, where traditional, univariate methodologies for

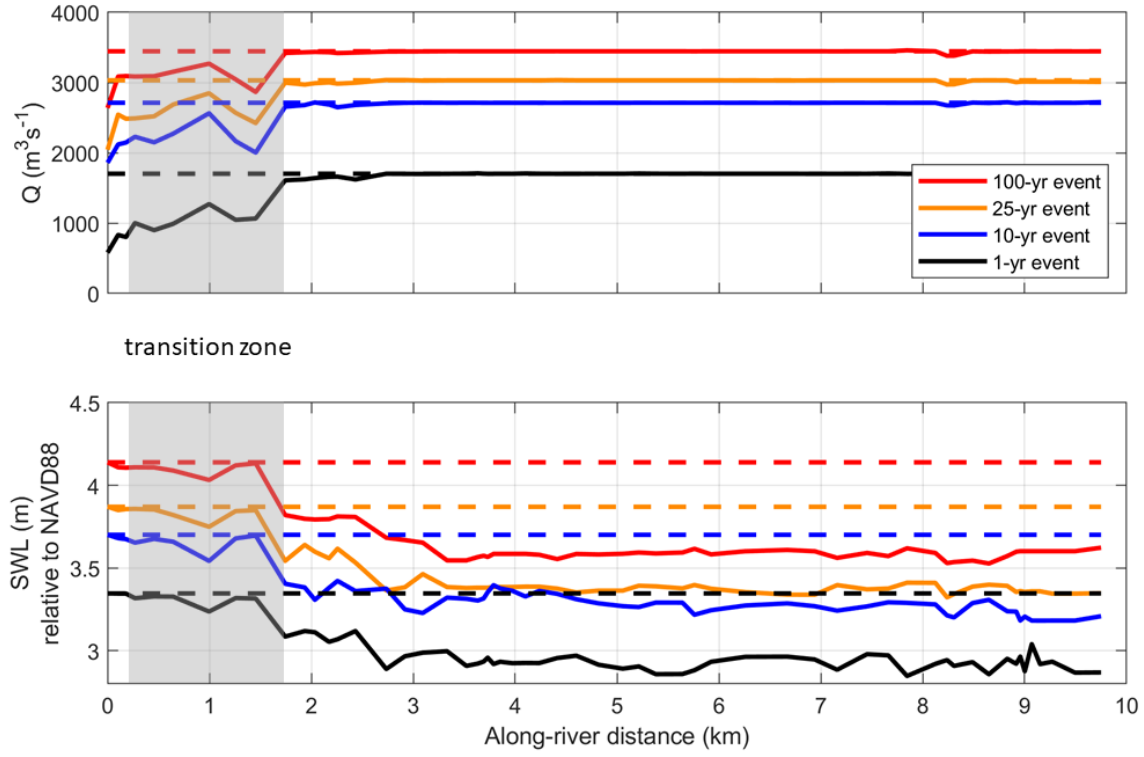

Figure 14. The ~~individual Q or SWL event~~ average forcing condition driving ~~the~~ along-river return levels at each transect where a) ~~annual~~ displays the Quillayute Q conditions and b) ~~100-yr event at specific~~ displays the SWL conditions. The dashed lines depict the univariate forcing conditions, where the along-river ~~locations~~return level is assumed to be driven by either Q or SWL. Red, orange, blue, and black lines represent the 100, 25, 10, and annual return level event. The grey shaded area represents a transition zone, where the water level is driven by a combination of SWL and Q events.

defining return level events are insufficient for defining water level return levels. Between river km ~~1.5 and 2.5~~1 and 2, we find that a range of SWL and Q ~~events~~ conditions drive all return level events, and water levels are driven by neither the univariate SWL or Q return level ~~drives the water level~~event. A similar flood zone transition was recently modeled numerically, and albeit for a single event, physically ~~demonstrated~~ demonstrates the importance of including multiple variables to reproduce accurate flooding (Bilskie and Hagen, 2018). Thus, flood hazard assessments on systems with multivariate forcings may misrepresent water level elevations for low probability events if only univariate variables are modeled. This has large implications for characterizing the risk to flooding, especially in the context of mapping flooding hazards. Furthermore, we show that return level water levels can occur over a range of combined extreme and non-extreme forcing in the flood transition zone. This

illustrates that in order to properly understand the impacts of compounding flooding, more than just design scenarios need to be considered for the proper assessment of risk.

Many of our results can be explained by dynamics that occur during interacting ocean and river flows. For example, a coincidence of high SWL and peak river discharge may induce blocking, where river-induced water levels are trapped upstream and either flood overbank or outlet to the ocean ~~when water~~ as the tide recedes (Kumbier et al., 2018; Chen and Liu, 2014). ~~While our ADCIRC~~ The outletting to the ocean as the tide recedes artificially inflates SWLs at the tide gauge, increasing water levels for days at a time and prolonging exposure to flooding. When subtracting a tide time series from this signal, storm surge would appear to be elevated at low tide. While the ADCSWAN simulation confirms the presence of this effect by matching the peak storm surge at low tide, our hybrid methodology only models steady flow scenarios. Thus, with co-occurring daily maximum SWL and discharge, ~~we~~ our model may miss certain dynamics important for flooding over unsteady conditions. ~~At low tide, a high river discharge may promote drainage of the floodwater into the ocean (Kumbier et al., 2018), increasing water levels for days at a time and prolonging exposure to flooding.~~ Furthermore, interactions between storm surge and river discharge may increase the overall elevation of the residual (Maskell et al., 2013). While beyond the scope of our present study, this unsteady characteristics are important to consider in future research.

Because sea level rise, along with other changes to the climate, will exacerbate the compounding effects of flood drivers (Moftakhari et al., 2017; Wahl et al., 2015), it is also important to consider the impact of changes to processes driving flooding events in the future (Zscheischler et al., 2018). By 2100, the likely range of relative sea level rise in the La Push area is projected to be between 18 and 80 cm, considering vertical land motion and ~~high and low~~ various emissions scenarios (Miller et al., 2018). The western Olympic Peninsula is projected to experience increased winter precipitation (Mote et al., 2013; Halofsky et al., 2011) which could subsequently increase either the frequency or intensity of high Q events along the Quillayute River. While we have characterized the spatial variability in extreme water levels in the present-day, there is a high likelihood changes in the future climate will shift the importance of these interacting processes.

7 Conclusions

This research illustrates the importance of considering a large number of forcing conditions to model compounding processes when evaluating extreme water levels. Here we find that in coastal settings, river discharge can be an important driver of high water levels measured in a tide gauge. We also find that the univariate, ~~forcing-driven~~ event-based return level event, like the 100-yr discharge, does not always match the ~~response~~ response-based return level, like the 100-yr water level. Furthermore, when processes compound, ~~the low probability water level~~ along-river return levels may be driven by events that are not considered extreme themselves. Probabilistic techniques allowing for the analysis of thousands to millions of combinations of events not captured in the observational record provides a ~~robust~~ characterization of where river, ocean, or the combination of the two, may be important for generating extreme events.

Overall, the hybrid merging of a statistical and numerical model provides a methodology for better understanding the drivers of flooding along the length of a river. While our model does not actively resolve the physical interaction of river and oceano-

graphic flow, it develops an approach for characterizing and extracting river-influenced water levels measured at tide gauges while robustly modeling the drivers of extreme along-river water levels. Understanding the dominant, spatially variable drivers of flooding events ~~now and into the future will ultimately increase the preparedness of the community of La Push~~will help coastal communities better understand their risks, which is important for increasing resilience to future events.

8 Data availability

Data can be made available by the authors upon request.

9 Author contribution

The study and methodology were conceived by KAS and PR. KAS carried out the analyses, produced the results, and wrote the manuscript under the supervision of PR. KAP carried out the analyses and produced the results of the ADCIRC simulations. KAP also developed the topography/bathymetry DEM as well as the geometric files for use in HEC-RAS. KAS, PR, KAP, and DFH all contributed by generating ideas, discussing results, and manuscript editing.

10 Competing interests

The authors declare that they have no conflict of interest.

Acknowledgements. Tide gauge records are available through the National Oceanic and Atmospheric Administration (NOAA) National Ocean Service (NOS) website and river discharge is available through the U.S Geological Survey (USGS) National Water Information System (https://waterdata.usgs.gov/wa/nwis/rt). Bathymetric and topographic data for DEM creation were obtained from NOAA's ~~Bathymetric Data viewer(DEMs) and DOGAMI's LiDAR download portal~~ Elevation Data viewer. Thank you to Michael Rossotto and Garrett Rasmussen for providing updated shapefiles of the Quileute Reservation boundaries. Thank you also to two anonymous reviewers whose comments improved the quality of this manuscript. This work was funded by the NOAA Regional Integrated Sciences and Assessments Program (NA15OAR4310145) and a contracted grant with the ~~Quileute tribe~~Quinault Treaty Area (QTA) tribal governments (Quinault Indian Nation, Hoh Indian Tribe, and Quileute Tribe).

References

Allan, J. C. and Komar, P. D.: Extreme storms on the Pacific Northwest coast during the 1997-98 El Niño and 1998-99 La Niña, Journal of Coastal Research, pp. 175–193, 2002.

Allan, J. C., Komar, P. D., and Ruggiero, P.: Storm Surge Magnitudes and Frequency on the Central Oregon Coast, in: Proc. Solutions to Coastal Disasters Conf, 2011.

Bevacqua, E., Maraun, D., Hobæk Haff, I., Widmann, M., and Vrac, M.: Multivariate statistical modelling of compound events via pair-copula constructions: analysis of floods in Ravenna (Italy), Hydrology and Earth System Sciences, 21, 2701–2723, 2017.

Bilskie, M. and Hagen, S.: Defining Flood Zone Transitions in Low-Gradient Coastal Regions, Geophysical Research Letters, 45, 2761–2770, 2018.

Bromirski, P. D., Flick, R. E., and Miller, A. J.: Storm surge along the Pacific coast of North America, Journal of Geophysical Research: Oceans, 122, 441–457, 2017.

Brunner, G. W.: HEC-RAS River Analysis System Hydraulic Reference Manual, Version 5.0, Tech. rep., 2016.

Bunya, S., Dietrich, J. C., Westerink, J., Ebersole, B., Smith, J., Atkinson, J., Jensen, R., Resio, D., Luettich, R., Dawson, C., et al.: A high-resolution coupled riverine flow, tide, wind, wind wave, and storm surge model for southern Louisiana and Mississippi. Part I: Model development and validation, Monthly Weather Review, 138, 345–377, 2010.

Butt, M. J., Umar, M., and Qamar, R.: Landslide dam and subsequent dam-break flood estimation using HEC-RAS model in Northern Pakistan, Natural Hazards, 65, 241–254, 2013.

Chelton, D. B. and Enfield, D. B.: Ocean signals in tide gauge records, Journal of Geophysical Research: Solid Earth, 91, 9081–9098, 1986.

Chen, W.-B. and Liu, W.-C.: Modeling flood inundation induced by river flow and storm surges over a river basin, Water, 6, 3182–3199, 2014.

Cheng, T., Hill, D., and Read, W.: The Contributions to Storm Tides in Pacific Northwest Estuaries: Tillamook Bay, Oregon, and the December 2007 Storm, Journal of Coastal Research, 31, 723–734, 2014.

Couasnon, A., Sebastian, A., and Morales-Nápoles, O.: A Copula-Based Bayesian Network for Modeling Compound Flood Hazard from Riverine and Coastal Interactions at the Catchment Scale: An Application to the Houston Ship Channel, Texas, Water, 10, 1190, 2018.

Czuba, J. A., Barnas, C. R., McKenna, T. E., Justin, G. B., and Payne, K. L.: Bathymetric and streamflow data for the Quillayute, Dickey, and Bogachiel Rivers, Clallam County, Washington, April–May 2010, vol. 537, US Department of the Interior, US Geological Survey, 2010.

Dalrymple, R. W., Zaitlin, B. A., and Boyd, R.: Estuarine facies models: conceptual basis and stratigraphic implications: perspective, Journal of Sedimentary Research, 62, 1992.

de Vries, H., Breton, M., de Mulder, T., Krestenitis, Y., Proctor, R., Ruddick, K., Salomon, J. C., Voorrips, A., et al.: A comparison of 2D storm surge models applied to three shallow European seas, Environmental Software, 10, 23–42, 1995.

Dietrich, J., Zijlema, M., Westerink, J., Holthuijsen, L., Dawson, C., Luettich Jr, R., Jensen, R., Smith, J., Stelling, G., and Stone, G.: Modeling hurricane waves and storm surge using integrally-coupled, scalable computations, Coastal Engineering, 58, 45–65, 2011.

Gianfagna, C. C., Johnson, C. E., Chandler, D. G., and Hofmann, C.: Watershed area ratio accurately predicts daily streamflow in nested catchments in the Catskills, New York, Journal of Hydrology: Regional Studies, 4, 583–594, 2015.

Goodell, C.: Breaking the HEC-RAS Code: A User's Guide to Automating HEC-RAS, h2ls, Portland, OR, 2014.

Graham, N. E. and Diaz, H. F.: Evidence for intensification of North Pacific winter cyclones since 1948, Bulletin of the American Meteorological Society, 82, 1869–1893, 2001.

Halofsky, J. E., Peterson, D. L., O'Halloran, K. A., and Hoffman, C. H.: Adapting to climate change at Olympic National Forest and Olympic National Park, Gen. Tech. Rep. PNW-GTR-844. Portland, OR: US Department of Agriculture, Forest Service, Pacific Northwest Research Station. 130 p, 844, 2011.

Horritt, M. and Bates, P.: Evaluation of 1D and 2D numerical models for predicting river flood inundation, Journal of Hydrology, 268, 87–99, 2002.

Horsburgh, K. and Wilson, C.: Tide-surge interaction and its role in the distribution of surge residuals in the North Sea, Journal of Geophysical Research: Oceans, 112, 2007.

Komar, P. D., Allan, J. C., and Ruggiero, P.: Sea level variations along the US Pacific Northwest coast: Tectonic and climate controls, Journal of Coastal Research, 27, 808–823, 2011.

Kumbier, K., Cabral Carvalho, R., Vafeidis, A. T., and Woodroffe, C. D.: Investigating compound flooding in an estuary using hydrodynamic modelling: a case study from the Shoalhaven River, Australia, Natural Hazards and Earth System Sciences, 18, 463–477, 2018.

Leonard, M., Westra, S., Phatak, A., Lambert, M., van den Hurk, B., McInnes, K., Risbey, J., Schuster, S., Jakob, D., and Stafford-Smith, M.: A compound event framework for understanding extreme impacts, Wiley Interdisciplinary Reviews: Climate Change, 5, 113–128, 2014.

Luettich Jr, R. A., Westerink, J. J., and Scheffner, N. W.: ADCIRC: An Advanced Three-Dimensional Circulation Model for Shelves, Coasts, and Estuaries. Report 1. Theory and Methodology of ADCIRC-2DDI and ADCIRC-3DL., Tech. rep., Coastal Engineering Research Center, Vicksburg MS, 1992.

Maskell, J., Horsburgh, K., Lewis, M., and Bates, P.: Investigating River–Surge Interaction in Idealised Estuaries, Journal of Coastal Research, 30, 248–259, 2013.

Mawdsley, R. J. and Haigh, I. D.: Spatial and temporal variability and long-term trends in skew surges globally, Frontiers in Marine Science, 3, 29, 2016.

Miller, I., Morgan, H., Mauger, G., T., N., R., W., D., S., M., W., and E., G.: Projected sea level rise for Washington state: A 2018 assessment, Tech. rep., A colloboration of Washington Sea Grant, University of Washington Climate Impacts Group, Oregon State University, University of Washington, and US Geological Survey. Prepared for the Washington Coastal Resilience Project, 2018.

Moftakhari, H., Schubert, J. E., AghaKouchak, A., Matthew, R., and Sanders, B. F.: Linking Statistical and Hydrodynamic Modeling for Compound Flood Hazard Assessment in Tidal Channels and Estuaries, Advances in Water Resources, 2019.

Moftakhari, H. R., Salvadori, G., AghaKouchak, A., Sanders, B. F., and Matthew, R. A.: Compounding effects of sea level rise and fluvial flooding, Proceedings of the National Academy of Sciences, 114, 9785–9790, 2017.

Mote, P. et al.: Climate: Variability and Change in the Past and the Future. Chapter 2, 25-40, 2013.

Odigie, K. O. and Warrick, J. A.: Coherence between Coastal and River Flooding along the California Coast, Journal of Coastal Research, 2017.

Olabarrieta, M., Warner, J. C., and Kumar, N.: Wave-current interaction in Willapa Bay, Journal of Geophysical Research: Oceans, 116, 2011.

Olbert, A. I., Comer, J., Nash, S., and Hartnett, M.: High-resolution multi-scale modelling of coastal flooding due to tides, storm surges and rivers inflows. A Cork City example, Coastal Engineering, 121, 278–296, 2017.

Razavi, S., Tolson, B. A., and Burn, D. H.: Review of surrogate modeling in water resources, Water Resources Research, 48, 2012.

Saleh, F., Ramaswamy, V., Wang, Y., Georgas, N., Blumberg, A., and Pullen, J.: A Multi-Scale Ensemble-based Framework for Forecasting Compound Coastal-Riverine Flooding: The Hackensack-Passaic Watershed and Newark Bay, Advances in Water Resources, 2017.

Serafin, K. A. and Ruggiero, P.: Simulating extreme total water levels using a time-dependent, extreme value approach, Journal of Geophysical Research: Oceans, 119, 6305–6329, 2014.

Serafin, K. A., Ruggiero, P., and Stockdon, H. F.: The relative contribution of waves, tides, and nontidal residuals to extreme total water levels on US West Coast sandy beaches, Geophysical Research Letters, 44, 1839–1847, 2017.

Serafin, K. A., Ruggiero, P., Barnard, P., and Stockdon, H. F.: The influence of shelf bathymetry and beach topography on extreme total water levels: Linking large-scale changes of the wave climate to local coastal hazard, Coastal Engineering, 2019.

Svensson, C. and Jones, D. A.: Dependence between extreme sea surge, river flow and precipitation in eastern Britain, International Journal of Climatology, 22, 1149–1168, 2002.

Sweet, W. V., Park, J., Gill, S., and Marra, J.: New ways to measure waves and their effects at NOAA tide gauges: A Hawaiian-network perspective, Geophysical Research Letters, 42, 9355–9361, 2015.

Tsimplis, M. and Woodworth, P.: The global distribution of the seasonal sea level cycle calculated from coastal tide gauge data, Journal of Geophysical Research: Oceans, 99, 16 031–16 039, 1994.

van den Hurk, B., van Meijgaard, E., de Valk, P., van Heeringen, K.-J., and Gooijer, J.: Analysis of a compounding surge and precipitation event in the Netherlands, Environmental Research Letters, 10, 035 001, 2015.

Vetter, O., Becker, J. M., Merrifield, M. A., Pequignet, A.-C., Aucan, J., Boc, S. J., and Pollock, C. E.: Wave setup over a Pacific Island fringing reef, Journal of Geophysical Research: Oceans, 115, 2010.

Wahl, T., Jain, S., Bender, J., Meyers, S. D., and Luther, M. E.: Increasing risk of compound flooding from storm surge and rainfall for major US cities, Nature Climate Change, 5, 1093–1097, 2015.

Ward, P. J., Couasnon, A., Eilander, D., Haigh, I. D., Hendry, A., Muis, S., Veldkamp, T. I., Winsemius, H. C., and Wahl, T.: Dependence between high sea-level and high river discharge increases flood hazard in global deltas and estuaries, Environmental Research Letters, 13, 084 012, 2018.

Weaver, R. and Luettich, Jr, R.: 2D vs. 3D storm surge sensitivity in ADCIRC: Case study of hurricane isabel, in: Estuarine and Coastal Modeling (2009), pp. 762–779, ASCE, 2010.

Williams, J., Horsburgh, K. J., Williams, J. A., and Proctor, R. N.: Tide and skew surge independence: New insights for flood risk, Geophysical Research Letters, 43, 6410–6417, 2016.

WRCC: Climate of Washington: Western Regional Climate Center website, https://wrcc.dri.edu/Climate/narrative$_w a.php$, 2017.

Yang, J., Townsend, R. D., and Daneshfar, B.: Applying the HEC-RAS model and GIS techniques in river network floodplain delineation, Canadian Journal of Civil Engineering, 33, 19–28, 2006.

Zheng, F., Westra, S., and Sisson, S. A.: Quantifying the dependence between extreme rainfall and storm surge in the coastal zone, Journal of Hydrology, 505, 172–187, 2013.

Zijlema, M.: Computation of wind-wave spectra in coastal waters with SWAN on unstructured grids, Coastal Engineering, 57, 267–277, 2010.

Zscheischler, J., Westra, S., Hurk, B. J., Seneviratne, S. I., Ward, P. J., Pitman, A., AghaKouchak, A., Bresch, D. N., Leonard, M., Wahl, T., et al.: Future climate risk from compound events, Nature Climate Change, p. 1, 2018.

Supplemental Information

Katherine A. Serafin[1,2], Peter Ruggiero[1], Kai A. Parker[3], and David F. Hill[3]

[1]College of Earth, Ocean, and Atmospheric Sciences, Oregon State University, Corvallis, OR, USA
[2]Department of Geophysics, Stanford University, Stanford, CA, USA
[3]College of Engineering, Oregon State University, Corvallis, OR, USA

Correspondence: Katherine A. Serafin (kserafin@stanford.edu)

1 Hydraulic model domain and setup

HEC-RAS model runs require detailed terrain information for the river network, including bathymetry and topography for the floodplains of interest. Topography data is sourced from a 2014 U.S Army Corps of Engineers (USACE) lidar survey (USACE, 2014). Bathymetry data is developed by blending two NOAA digital elevation models (DEM): National Geophysical Data Center's (NGDC) La Push, WA tsunami DEM (1/3 arc second; NGDC (2007)) and the coastal relief model (3 arc seconds; NGDC (2003)). These datasets, however, do not accurately resolve the channel depths of the Quillayute River inland of the coast, so a 2010 US Geological Survey (USGS)-conducted bathymetric survey of the river is also blended into the DEM (Czuba et al., 2010).

In 2010, depths of along-river cross sections and an 11 km long longitudinal profile from the Bogachiel River to the mouth of the Quillayute River were surveyed (Czuba et al., 2010). The survey of the longitudinal river profile also recorded the elevation of the water surface. Ideally, the collected bathymetry dataset would be merged directly into the existing DEM. The Quillayute River, however, is uncontrolled and meanders over time, producing a variation in the location of the main river channel between the DEM and the high-resolution USGS-collected bathymetric data. Therefore, the USGS bathymetric profiles are adjusted to match the location of the DEM channel. While a product of multiple datasets and processing steps, the final DEM provides bathymetric/topographic data with the most up-to-date channel depths for the Quillayute River (Figure 6, main text).

A series of 58 transects are extracted from the DEM using HEC-GeoRas (Ackerman, 2009) and written into a geometric data file for input into HEC-RAS. Each river transect extends across the floodplain to the 10 m contour, where applicable. Otherwise, each transect terminates at the highest point landward of the river. Because HEC-RAS computes energy loss at each transect via a frictional loss based on the Manning's equation, Manning's coefficients, an empirically derived coefficient representing resistance of flow through roughness and river sinuosity, are selected for the river channel and the floodbanks. In-channel Manning's coefficients are tuned to calibrate the model's resulting water surface elevations with that of the observed water surface data. Manning's coefficients for the rest of the computational domain (e.g., anything overbank) are estimated using 2011 Land Cover data from the Western Washington Land Cover Change Analysis project (NOAA, 2012) and visual inspection of aerial imagery and range from 0.04 (cleared land with tree stumps) - 0.1 (heavy stands of timber/medium to dense brush). These values are extracted from the HEC-RAS Hydraulic Reference Manual, Table 3-1 (Brunner, 2016). Model

domain boundary conditions are chosen as the water surface elevation at the tide gauge (m; downstream boundary) and river discharge from a combination of records representing the Quillayute River watershed (m^3s^{-1}; upstream boundary).

1.1 HEC-RAS model validation

In order to determine the dominant inputs to Quillayute River discharge, combined estimates of the Sol Duc and Calawah Rivers are compared to measurements taken on the Quillayute River in May 2010 (Czuba et al., 2010). Combined discharge estimates from the Sol Duc and Calawah rivers underpredict streamflow in the Quillayute River by approximately 33%. An area scaling watershed analysis (Gianfagna et al., 2015), described in the main text, found that the Bogachiel and Calawah Rivers had similar contributions. Thus the Calawah river is scaled by a factor of 2.09 to represent the Bogachiel River. Combined discharge estimates from the Sol Duc River and Bogachiel River, representing the Quillayute River, are also compared to the Quillayute discharge measurements taken during the 2010 survey. Using this methodology, the discharge estimates of the Quillayute River fall within the uncertainty of the discrete USGS measurements in most cases (Table 1).

The longitudinal measured water surface profile allows for the verification and calibration of HEC-RAS modeled water surface elevations on the day of the survey (Figure 1). HEC-RAS is run using discharge of the watershed-scaled Bogachiel River as the upstream boundary condition during the hour of the field survey and this discharge is combined with a lateral inflow from the Sol Duc River around river km 8.5. Manning's coefficients within the main channel of the Quillayute River are calibrated to best represent the water surface elevation on the day of the USGS longitudinal survey. Final Manning's coefficients range from to 0.005 to 0.1, and are on average 0.025.

The final calibrated HEC-RAS model produces a water surface elevation with an average bias less than 1% (less than 1 cm) and an average standard deviation of approximately 5% (7.5 cm). The maximum difference between the two water surfaces is approximately 14 cm (20%). The percent difference between the depth of the observed and modeled water surface is almost always less than 10% (Figure 1).

2 Tide gauge processing

The continuous La Push tide gauge record begins in 2004, recording 12 years of water levels. This record, however, does not capture the extreme water levels occurring during the 1982/83 and 1997/98 El Niños. Therefore, water levels from the La Push tide gauge are merged with water levels from the Toke Point tide gauge (beginning in 1980, NOAA station 9440910) to create a combined water level record representing a larger range of extreme conditions. η_A and η_{SE}, water level components deterministic to the La Push tide gauge, are extended to 1980. Water level components influenced by regional or local forcings like η_{MMSLA} and η_{SS}, are compared before combining. η_{MMSLA} between the Toke Point and La Push tide gauges are similar, so Toke Point η_{MMSLA} are appended to the beginning of the La Push η_{MMSLA}. Toke Point, however, has slightly higher magnitude η_{SS} than La Push and there is a noticeable offset in the highest η_{SS} peaks. A correction is thus applied to the Toke Point η_{SS} before appending it to the beginning of the La Push η_{SS}. η_{MSL} is extended back to 1980 using relative sea level rise trends for the region. Once the two tide gauges are merged, the combined hourly tide gauge record extends from

Table 1. Quillayute River discharge measurements from the USGS survey (Czuba et al., 2010) compared to the Quillayute River discharge estimates computed by adding the Sol Duc USGS gauge measurements with the Bogachiel River discharge, estimated via scaling of the Calawah River gauge measurements. The parenthesis in the last column is the standard deviation of USGS survey measurements (m^3s^{-1}).

Date of Survey	Sol Duc (m^3s^{-1})	Calawah (m^3s^{-1})	Bogachiel (m^3s^{-1}) (estimated)	Quillayute (m^3s^{-1}) (estimated)	Quillayute (m^3s^{-1}) (measured)
4/20/2010	52	28	58	110	116 (7)
4/21/2010a	48	25	53	101	108 (1)
4/21/2010b	48	25	52	100	103 (3)
4/21/2010c	46	24	50	96	107 (1)
5/4/2010a	73	69	144	217	220 (5)
5/4/2010b	70	66	137	207	207 (4)
5/5/2010	59	51	107	166	170 (3)
5/6/2010	50	40	84	134	136 (3)

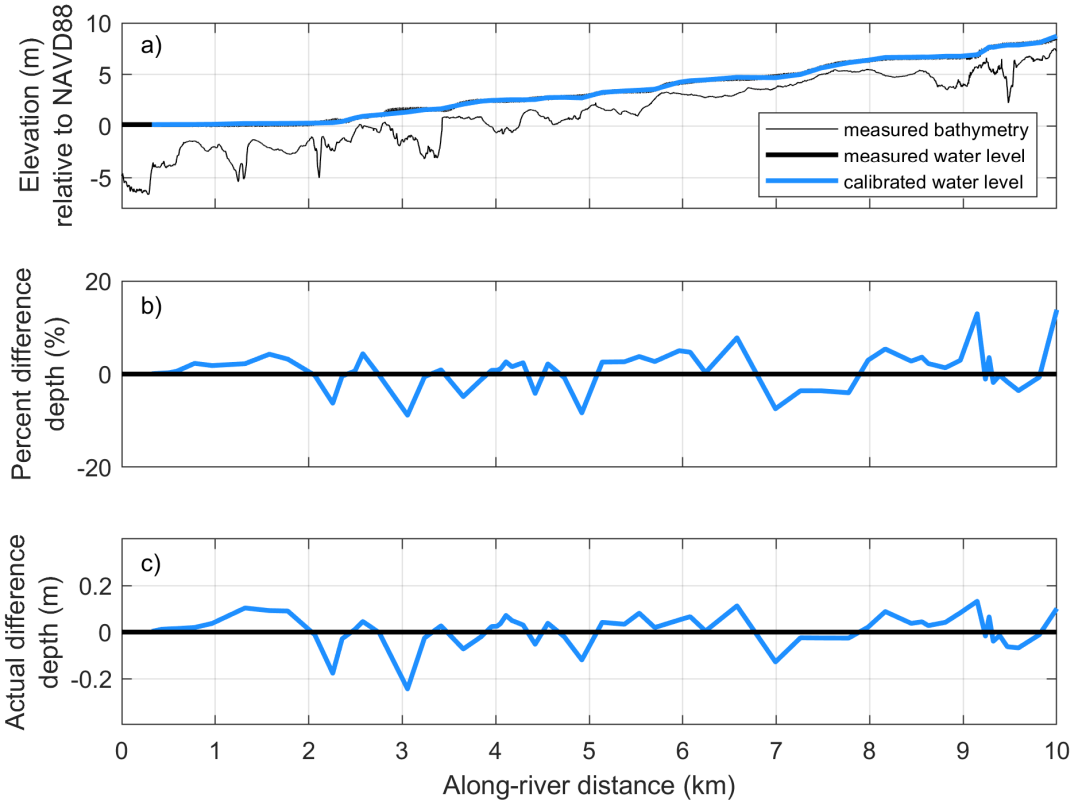

Figure 1. a) Bathymetry and longitudinal profile from the Bogachiel River to the mouth of the Quillayute River surveyed by the USGS in May of 2010 (black). The longitudinal water level for the calibrated HEC-RAS model is depicted in blue. b) Percent difference between the measured (black) and HEC-RAS modeled (blue) water level. c) Actual difference between the measured (black) and HEC-RAS modeled (blue) water level.

1980 - 2016 and is 97% complete. Discharge measurements sampled at 15 minute intervals for the Calawah and Sol Duc rivers are interpolated to hourly increments to match the timing of the SWL measurements.

2.1 Removal of river-influence from the oceanographic signal

Storms tend to influence large stretches of coastline at once, and while site-specific variations in the coastline or distance from storm can drive local variations in the amplitude of η_{SS}, the overall η_{SS} signal is fairly coherent across regional tide gauges across the PNW. The river-influenced water levels are therefore isolated and removed from the La Push η_{SS} record by developing a relationship between the La Push η_{SS} and a regionally-averaged η_{SS}.

η_{SS} decomposed from the Neah Bay, Westport, Astoria, Garibaldi, and South Beach tide gauges are averaged each hour to create a regional η_{SS} record (black line; Figure 2). The standard deviation (σ) of the available η_{SS} records at each hour is used

to represent the variability of η_{SS} due to local effects at each station. η_{SS} at La Push that are larger than the regional average + 2.5σ are considered anomalous to the region, and defined as river-influenced water levels (η_{Ri}). Observations flagged as larger than the regional average + 2.5σ (dashed line; Figure 2) were replaced with the regional average + σ. A value of + σ was chosen to minimize jumps in time series when substituting in a smoother dataset. While this methodology does not remove all the effects of η_{Ri} in the η_{SS} signal, it captures the majority of anomalous water levels driven by high discharge events.

η_{Ri} is produced from the difference between the original La Push η_{SS} and the η_{SS} modified described above which removes η_{SS} anomalous events. η_{Ri} occurring during low discharge events (here low is defined as less than 10 m^3s^{-1}, the approximate summer average discharge) is added back into the La Push η_{SS}, as it is likely not driven by river forcing. After η_{Ri} was removed from the η_{SS} signal, it is saved as a time series of river-forced water level events.

Extreme Hs and Q events at the Calawah River are determined using the Peak Over Threshold approach, where all independent daily maximum events over a defined threshold are selected. Threshold excesses are fit to non-stationary Generalized Pareto distributions, which include seasonality as a covariate. Both variables are transformed to approximately Fréchet margins. A bivariate logistic model is then used to model the dependency between the variables. To simulate, random numbers are sampled from a uniform distribution and mapped to each variable's prescribed Fréchet cumulative probability distribution function. Based on the probability of occurrence of the transformed value, the estimate is transformed back to the physical scale using the Generalized Pareto distribution if extreme, dependent on the variable's threshold. If not extreme, the estimate is transformed back to the physical scale using monthly-varying Gaussian copulas. This technique generates a synthetic record of Q at the Calawah River gauge that is seasonally varying, related to larger-scale climate variability through wave height (essentially as a proxy for storms), and carries the same dependency between variables as the observational record. Q is then multiplied by 2.09 to represent inflow from both the Bogachiel and Calawah rivers.

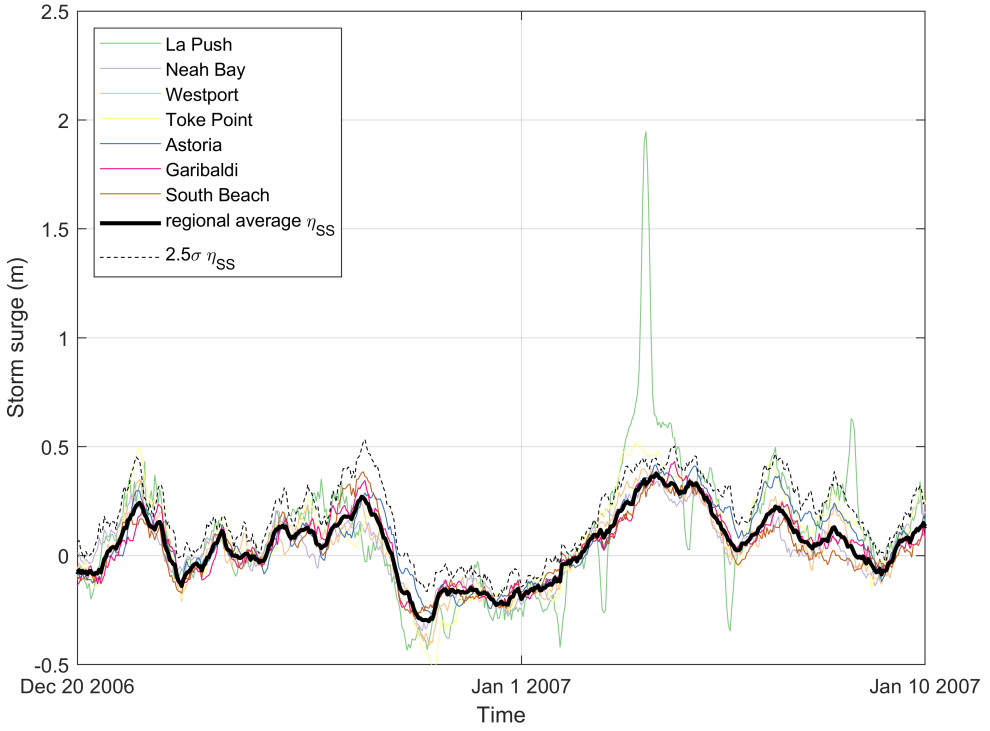

Figure 2. A comparison of storm surge (η_{SS}) decomposed from all tide gauges along the northern Washington to central Oregon coastline. The solid, black line depicts the regional average of all of the η_{SS} signals, while the dashed black line represents the regional average η_{SS} + 2.5*σ of all η_{SS} in the region. When the La Push η_{SS} exceeds the regional average η_{SS} + 2.5*σ it is removed from the record and considered river influence.

References

Ackerman, C. T.: HEC-GeoRAS; GIS Tools for support of HEC-RAS using ArcGIS, Tech. rep., United States Army Corps of Engineers, Davis, 2009.

Brunner, G. W.: HEC-RAS River Analysis System Hydraulic Reference Manual, Version 5.0, Tech. rep., 2016.

Czuba, J. A., Barnas, C. R., McKenna, T. E., Justin, G. B., and Payne, K. L.: Bathymetric and streamflow data for the Quillayute, Dickey, and Bogachiel Rivers, Clallam County, Washington, April–May 2010, vol. 537, US Department of the Interior, US Geological Survey, 2010.

Gianfagna, C. C., Johnson, C. E., Chandler, D. G., and Hofmann, C.: Watershed area ratio accurately predicts daily streamflow in nested catchments in the Catskills, New York, Journal of Hydrology: Regional Studies, 4, 583–594, 2015.

NGDC: U.S. Coastal Relief Model - Northwest Pacific. National Geophysical Data Center, NOAA, https://www.ncei.noaa.gov/metadata/geoportal/rest/metadata/item/gov.noaa.ngdc.mgg.dem:288/html, https://doi.org/doi:10.7289/V5H12ZXJ, 2003.

NGDC: La Push, Washington 1/3 arc-second MHW Coastal Digital Elevation Model, https://data.noaa.gov//metaview/page?xml=NOAA/NESDIS/NGDC/MGG/DEM/iso/xml/247.xml&view=getDataView&header=none, 2007.

NOAA: C-CAP Washington 2011-Era Land Cover Metadata, https://coast.noaa.gov/ccapatlas/, 2012.

USACE: 2014 USACE NCMP Topobathy Lidar: Washington, https://coast.noaa.gov/dataviewer/#/lidar/search/where:ID=6263, 2014.